Journal of Power Sources 441 (2019) 227175

Contents lists available at ScienceDirect

Journal of Power Sources

journal homepage: www.elsevier.com/locate/jpowsour

Review article

Challenges and development of composite solid-state electrolytes for high-performance lithium ion batteries

Fei Lv [a], Zhuyi Wang [a,**], Liyi Shi [a], Jiefang Zhu [b], Kristina Edström [b], Jonas Mindemark [b], Shuai Yuan [a,c,*]

[a] Research Centre of Nanoscience and Nanotechnology, Shanghai University, Shanghai, 200444, China
[b] Department of Chemistry - Ångström Laboratory, Uppsala University, SE-751 21, Uppsala, Sweden
[c] Emerging Industries Institute, Shanghai University, Jiaxing, Zhejiang, 314006, China

ARTICLE INFO

Keywords:
Composite solid-state electrolytes
Li^+ ion transportation
Interface issues
Lithium ion batteries

ABSTRACT

The safety concerns and the pursuit of high energy density have stimulated the development of high-performance solid-state lithium ion batteries. Therefore, the key component in solid-state lithium batteries, i.e. the solid-state electrolytes, also has attracted tremendous attention due to its non-flammability and good adaptability to high-voltage cathodes/lithium metal anodes. An in-depth understanding of the existing problems of solid-state electrolytes and proposed strategies for addressing these problems is crucial for the efficient design of high-performance solid-state electrolytes. In this review, we systematically summarized the current limitations of composite solid-state electrolytes and efforts to overcome them, and gave some proposals for the future perspectives of solid-state electrolytes with the aim to provide practical guidance for the researchers in this area.

1. Introduction

Driven by the rapid development of new energy storage solutions for the automotive industry, lithium ion batteries (LIBs) are being developed towards higher energy density, higher safety and longer life [1–3]. However, conventional LIBs with liquid electrolytes are still confronted with severe safety hazard caused by the electrolyte leakage and irreversible decomposition [4]. In addition, the energy density of the existing high nickel-content cathode/silicon-carbon anode system has reached a limit of ~300 Wh kg^{-1}, which is not enough to satisfy the requirements on the next generation LIBs for new electric vehicles [5,6]. Therefore, the safety concerns and the pursuit of high energy density have stimulated the interests for high performance all-solid-state LIBs [7,8]. In addition, solid-state LIBs are easier to develop toward miniaturization and flexibility, and therefore are more suitable as the power supply of flexible devices such as penetrable batteries, wearable mobile phone, flexible screen etc. [9]. Moreover, Li–S batteries and Li–O_2 batteries equipped with solid-state electrolytes are of great significance for the sharply improvement of energy density, which has received more and more attention [10,11].

The solid-state electrolytes (SSEs), as one key component in all-solid-state lithium metal batteries, has the characteristics of non-flammability, high temperature resistance and non-volatilization, which make it possible to avoid electrolyte leakage and short circuit in traditional LIBs with liquid electrolytes, and therefore eradicates the hidden danger of safety [12,13]. In addition, the wider electrochemical window of SSEs will make it more adaptive to the high-voltage cathode materials [14,15]. At the same time, the solid-state electrolytes may also have better compatibility with lithium metal anodes. This better adaptability to high-voltage cathode materials and lithium metal anodes will greatly increase the energy density of batteries [14].

However, there are still many problems existing in the solid-state electrolytes, such as poor electrodes/electrolyte interface contact, low ion conductivity and electrochemical stability. According to several kinds of solid-state electrolytes developed at present, the solid-state polymer electrolytes (mainly PEO and its derivatives) can form good interface contact with electrodes, but their ionic conductivity at room temperature are usually very low and the electrochemical windows are limited [16,17]. Therefore, they have difficulties to match the high-voltage cathodes, and most polymer-based batteries are therefore still based on the $LiFePO_4$ cathode and often operate at elevated temperature (60–80 °C), which limits the increase in energy density of

* Corresponding author. Research Centre of Nanoscience and Nanotechnology, Shanghai University, Shanghai, 200444, China.
** Corresponding author.
E-mail addresses: bamboo2009@shu.edu.cn (Z. Wang), s.yuan@shu.edu.cn (S. Yuan).

https://doi.org/10.1016/j.jpowsour.2019.227175
Received 19 July 2019; Received in revised form 8 September 2019; Accepted 18 September 2019

solid-state batteries [18,19]. Although polyacrylonitrile (PAN) based solid-state polymer electrolytes have high oxidation resistance potential and can match high-voltage cathode materials, some researches have shown that nitrile-based polymers are unstable in contact with lithium metal leading to severe side reactions, and their low room temperature ionic conductivity and poor mechanical performance also limit their application [16,20]. Some methods such as adding low-molecular-weight liquid plasticizers or designing high-salt concentration polymer electrolytes were usually used to enhance the ionic conductivity of solid-state polymer electrolytes. But these methods are unfavorable for the mechanical properties and stability of the electrolytes [21,22].

Compared to solid-state polymer electrolytes, inorganic solid-state electrolytes usually have high room temperature ionic conductivity in the order of 10^{-3}-10^{-4} S cm^{-1} and high Li^+ ion transference number [9,23]. Oxide-based or sulfide-based solid-state electrolytes are two kinds of typical inorganic solid-state electrolytes. Some sulfide-based solid-state electrolytes even have ionic conductivity close to or higher than that of liquid electrolytes, but they are very sensitive to exotic environment [24,25]. The oxide-based solid-state electrolytes are usually relatively stable in the atmosphere, but they all exist different limitations preventing their application. For example, both sodium superionic conductors (NASICON) and perovskite Li^+ ion conductors possess bad chemical stability to Li metal anode [26,27]. Garnet is stable when contacting with Li metal, but they are sensitive to water and CO_2 in the air to form side-products deposited on the surface [28]. Furthermore, a common drawback for inorganic solid-state electrolytes is their rigidity and brittleness leading to poor electrodes/electrolyte interface contact, which is the main obstacle to the practical application [29].

Considering the limitations of a single component electrolyte, composite solid-state electrolytes combining the advantages of two or more different components seem to be an effective strategy to solve the above problems. Due to the synergistic effects between different components (polymer and inorganic filler [30], polymer and polymer [31,32], etc.), composite solid-state electrolytes are expected to demonstrate satisfactory comprehensive properties and achieve the synergistic effects of 1 + 1 being more than 2, which has become an important direction for the development of new electrolytes [33].

The key of an all-solid-state lithium battery is to design and prepare with (1) good Li^+ ion transport ability and negligible electronic

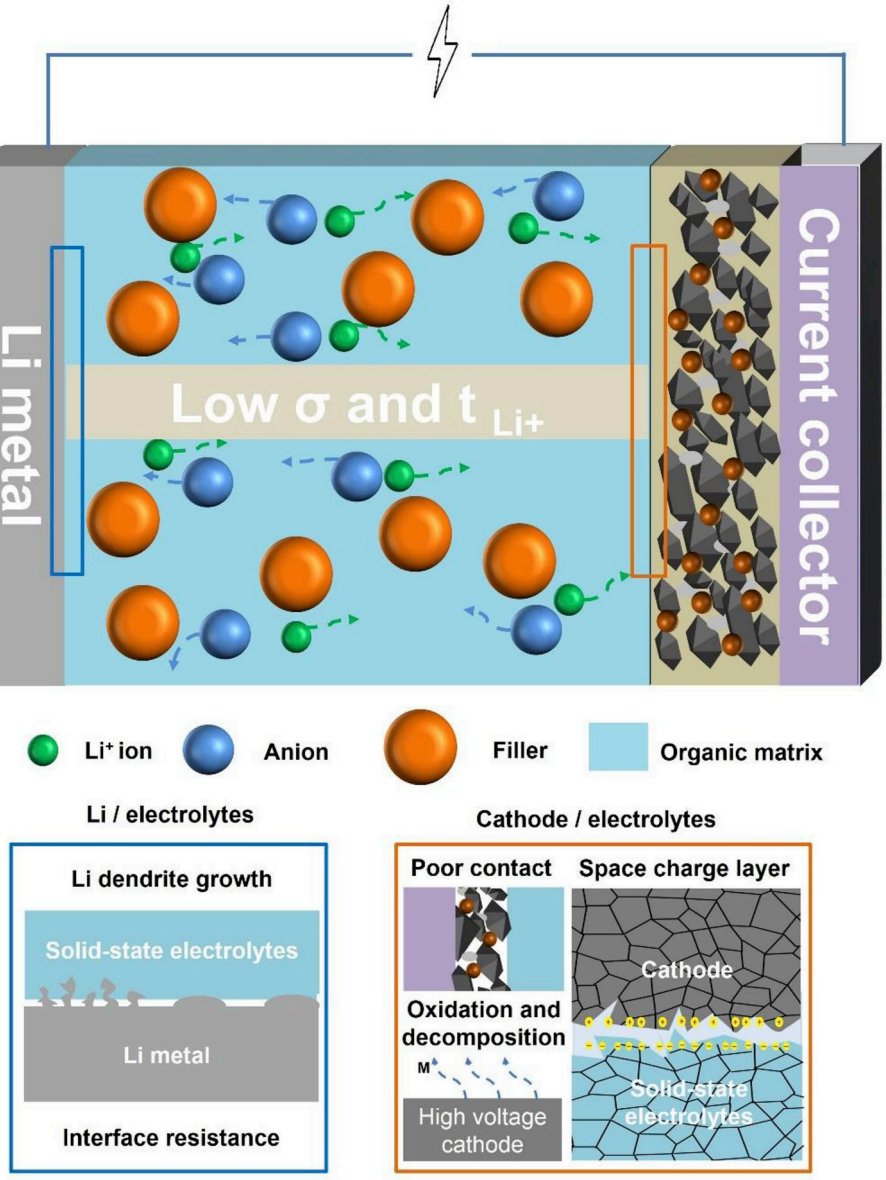

Fig. 1. Challenges of composite solid-state electrolytes: low ionic conductivity (σ) and Li^+ ion transference number (t_{Li+}), and electrodes/electrolytes interface issues.

conductivity at room temperature or even low temperature, (2) wide electrochemical stability window and chemical stability to Li metal anode, (3) favorable mechanical strength and flexibility, (4) excellent electrodes/electrolyte interface properties, (5) cost-effective and environmentally friendly. This review aims to highlight (i) the key existing issues for solid-state electrolytes, (ii) recent strategies and advances in addressing these issues, and (iii) possible directions for targeting high-performance composite solid-state electrolytes.

2. Challenges of composite solid-state electrolytes

Although composite solid-state electrolytes have great potential to be a substitute for traditional liquid electrolytes, many bottlenecks still need to be broken through in order to realize their application in solid-state LIBs (Fig. 1).

2.1. Ionic transport in composite electrolyte

The ionic conductivity (σ) and Li^+ ion transference number (t_{Li+}) are two pivotal variables evaluating Li^+ ion transport ability in composite solid-state electrolytes [34,35]. Currently, many works have been able to achieve an ionic conductivity of above 10^{-4} S cm^{-1} at room temperature. In contrast, less attention has been paid to the Li^+ ion transference number, which is usually below 0.5. In this condition, the total ionic conductivity is mainly contributed to anion motion, and the accumulation of anions at the electrode surface would result in a formation of a concentration gradient which induce a large concentration polarization [34,36]. Some strategies have been developed, such as blocking or immobilizing the anions by specific sandwich architectures to achieve high Li^+ ion transference number, but often at the expense of ionic conductivity [37–39]. Introducing polymer hosts that interact more weakly with the Li^+ ion than PEO has also been shown to increase the Li^+ ion transference number [40]. However, achieving the trade-off between ionic conductivity and Li^+ ion transference number, and obtain solid-state electrolytes with both excellent ion conductivity and high Li^+ ion transference number is still a big challenge.

Different from single component polymer or inorganic electrolytes, the composite electrolyte is a complex multi-component and multi-interface system [41]. As a result, the pathways for Li^+ ion transport is significantly different from that of homogeneous electrolytes system [42,43]. The ratio between different components and the electrolyte architecture regulate the Li^+ ion transport path ways, and it has therefore great impact on the Li^+ ion transport velocity [42,44,45]. Better understanding the mechanism for Li^+ ion transport in composite solid-state electrolytes will provide more insights into the rational design of solid-state electrolytes.

2.2. Electrodes/electrolyte interfacial issues

The electrodes/electrolyte interfacial issues are key factors affecting the electrochemical performances of all solid-state LIBs [14,46]. The contact resistance of the electrode/solid-state electrolyte interface is much larger than that of the electrode/liquid electrolyte interface, and the volume variation of electrodes during cycling in a solid-state battery may also cause contact failure. Meanwhile, the interface instability caused by side reactions between the electrodes and electrolytes also has adverse effects on the cycle performance and rate capability of batteries [3,47].

The diversity in the composition and structure of composite electrolytes allows for better electrodes/electrolyte interface design, according to the characteristics of electrodes, to improve the electrodes/electrolyte interface stability and reduce interface impedance, which is the key to push solid-state LIBs toward practical applications.

3. Efforts to overcome current obstacles

Over the past few decades, researchers have made great progress to overcome the limitations of composite solid-state electrolytes on the Li^+ ion transport and electrodes/electrolyte interface issues. We divide this part into four sections, illustrating the efforts made to enhance the ionic conductivity and Li^+ ion transference number, as well as stabilize electrodes/electrolyte interfaces.

3.1. Ionic conductivity

Since Wright et al. found that polymers based on ethylene oxide (EO) has the advantage of good ionic conduction when interacting with alkali metal ions, polyethylene oxide (PEO) has become the primary solid-state electrolytes to be applied in lithium-based batteries [48,49]. But the low ionic conductivity of PEO at room temperature limits its practical application [40]. Later, it was found that dispersing inorganic compounds in the polymer matrix reduces the crystallinity of PEO and therefore the ionic conductivity improves. Such findings aroused a flurry of interest in composite solid-state electrolytes [50,51].

3.1.1. Fillers with 0D particles

The conduction of Li^+ ion in PEO is based on the thermal motion of EO chains. Its practical application, however is usually at elevated temperatures due to its high crystallinity ($T_m > 60\,^{\circ}C$) [16]. In early stage, researchers found that introducing some 0D ceramic particles such as TiO_2, Al_2O_3, SiO_2 and ZrO_2 into the polymer matrix could reduce the crystallinity of PEO which facilitate the motion of the polymer chains, and therefore improve the ionic conductivity by 1–2 orders of magnitude [52–56].

Normally, the inert ceramic fillers are not involved in the Li^+ ion conducting process, so it would be more advantageous to use ion-conducting fillers that can provide additional lithium transport possibilities, which could further enhance the ionic conductivity [50,55,57]. The earliest used Li^+ ion conducting fillers is Li_3N, which was added into PEO leading to considerably improved ionic conductivity [58]. Later, a growing attention has been paid to ionically conducting inorganic ceramics such as $Li_{0.33}La_{0.557}TiO_3$ (LLTO) [59], $Li_7La_3Zr_2O_{12}$ (LLZO) [60] and $Li_{1+x}Al_xGe_{2-x}(PO_4)_3$ (LAGP) [61,62], and great efforts have been made by optimizing the microstructure and loading ratio of inorganic ceramic particles to maximize their advantages in two-phase or multi-phase composite solid-state electrolytes. Li et al. investigated the effects of particle size of Ta-doped LLZO (LLZTO) on the ionic conductivity of LLZTO/PEO composite electrolytes [63]. They found that the composite electrolytes containing ~40 nm LLZTO particles exhibited conductivity nearly two orders of magnitude larger than those with micron size due to the percolation behavior along the interface of LLZTO/PEO. These results signify the importance of tuning the Li^+ ion transport in the phase interfaces.

The loading ratio of inorganic ceramic Li^+ ion conductor in composite electrolytes have great impact on the ionic conductivity. According to the “percolation model”, the conductivity firstly increases with the fraction of fillers in the composite solid-state electrolytes and then decreases when the filler fraction increases to a critical point [64,65]. The conductivity reduction results from the blocking effects of particles on Li^+ ion conduction at high loading ratio. The effects of the fraction of ceramic $Li_7La_3Zr_2O_{12}$ (LLZO) phase in the LLZO/PEO composites on the ionic conductivity were investigated by studying the local structural environments and dynamics of Li^+ ion via solid-state NMR [45]. As revealed in Fig. 2a, the ion transport pathways gradually transition from PEO matrix to percolated LLZO network with increasing LLZO content to a critical point. The composites with <20 wt% LLZO loading showed the rise in the concentration of active Li^+ ion with increasing the LLZO content. But with the further increase of LLZO content, the opposite effects of LLZO on the ionic conductivity appeared due to the blockage of Li^+ ion conduction channels by the loose LLZO

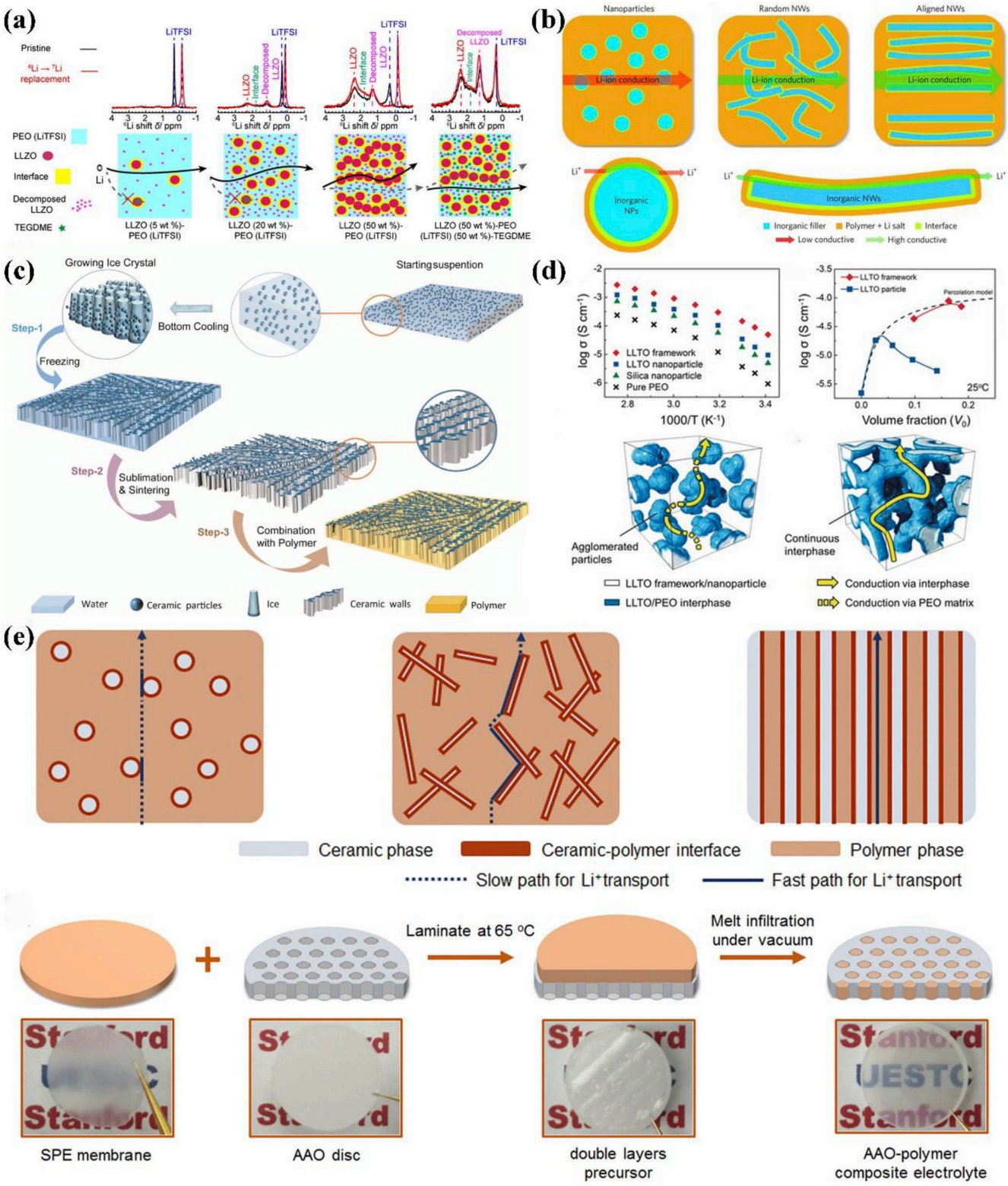

Fig. 2. (a) Schematic images of Li^+ ion pathways and ^6Li NMR comparison of pristine and cycled in composite solid-state electrolyte with various LLZO concentrations (Reproduced with permission [45]). (b) The comparison of possible Li^+ ion conduction pathways in composite polymer electrolytes with different fillers: nanoparticles, random nanowires and vertical nanowires (Reproduced with permission [66]). (c) Schematics of fabrication procedures of composite electrolyte with vertically aligned LAGP particles by ice-templated method (Reproduced with permission [69]). (d) Ionic conductivity of various composite electrolyte and percolation model curve as well as the possible Li^+ ion conduction mechanism with different structure: agglomerated nanoparticles and 3D continuous framework (Reproduced with permission [70]). (e) Design strategy, fabrication procedures of short-range ordered Li^+ ion conducting ceramic−polymer interface (Reproduced with permission [75]).

particles with lower conductivity.

3.1.2. Fillers with randomly distributed or well-aligned 1D structure

The morphology of inorganic fillers may lead to different inorganic-polymer interfacial geometries, which could significantly affect the enhancement of the ionic conductivity in the composite electrolytes. For ceramic nanoparticles with low aspect ratios, the ions transport pathways are short-ranged and isolated, and therefore the ionic conductivity enhancement is limited [43,45]. In comparison, one-dimensional (1D) inorganic ceramic nanostructures can create continuous ion transport pathways with much longer distances and minimize the inter-particles junctions, thereby facilitating Li^+ ion transport. For example, the composite electrolyte of polyacrylonitrile (PAN)/$LiClO_4$ incorporated with 15 wt % $Li_{0.33}La_{0.557}TiO_3$ nanowires exhibited an ionic conductivity as high as 2.4×10^{-4} S cm^{-1} at room temperature, which was much higher in comparison to the state-of-the-art composite electrolytes with ceramic nanoparticles at the same blending level [59]. In the subsequent work, the authors designed a composite polymer electrolyte with vertically aligned LLTO nanowires in a PAN polymer matrix by photolithography [66]. As shown in Fig. 2b, the replacement of disordered nanowires with well-aligned nanowires in the polymer matrix created another order of magnitude in enhancement of the ionic conductivity. The large conductivity enhancement is ascribed to a fast ion-conducting pathway without crossing junctions on the surface of the aligned nanowires.

Such structural design has also been applied to PEO-based composite electrolytes [67–69]. Yang et al. prepared vertically aligned $Li_{1.5}Al_{0.5}Ge_{1.5}(PO_4)_3$ (LAGP) ceramic nanoparticles by an ice-template method, which was filled with PEO/LiTFSI to obtain the composite electrolyte (Fig. 2c) [69]. The vertically aligned LAGP interface provided continuous and fast Li^+ ion transport channels, while the PEO matrix made the composite electrolyte flexible and led to better contact to the electrodes. The as-prepared composite electrolyte showed an ionic conductivity of 1.67×10^{-4} S cm^{-1} at room temperature and 1.11×10^{-3} S cm^{-1} at 60 °C, which was 6.9 times as much as that of randomly distributed particles.

3.1.3. Fillers with continuous 3D structure

In order to provide continuous ionic conduction pathways, inorganic fillers with a three-dimensional (3D) network of interconnected channels have attracted more and more attention. Yu et al. fabricated LLTO/PEO and LLZO/PEO composite electrolytes by three-dimensional (3D) nanostructured hydrogel-derived LLTO [70] and LLZO [71] frameworks embedded with a PEO/LiTFSI ionic conduction polymer network, achieving an enhanced Li^+ ion conductivity close to 10^{-4} S cm^{-1} at room temperature (Fig. 2d). Hu et al. synthesized a 3D $Li_{6.4}La_3Zr_2Al_{0.2}O_{12}$ network framework through electrostatic spinning and high temperature annealing. This 3D network was then filled with a PEO/LiTFSI solution [72]. The as-prepared composite solid-state electrolytes displayed a high ionic conductivity of 2.5×10^{-4} S cm^{-1} at room temperature. It can be attributed to the interconnected 3D inorganic framework, in which a continuous ceramic/polymer phase interface was formed for Li^+ ion transport.

3.1.4. Fillers with optimized interfacial properties

Conventional composite solid-state electrolytes are usually fabricated by blending different components, without any chemical interaction occurring between them. However, the void between two different phases will barrier the ion transfer. The surface of fillers should be very well wetted by the continuous phase to eliminate the influence of voids. The ionic conductivity of composite solid-state electrolytes can be tuned by modifying surface chemistry of the ceramic phase, optimizing the polymer/lithium salts system, or by varying the ceramic/polymer specific interfacial area. For example, the compatibility and dispersity of LLZTO in the PEO matrix can be improved by precoating of LLZTO with dopamine, leading to a significant enhancement of the ionic conductivity of composite solid-state electrolytes from 6.3×10^{-5} S cm^{-1} to 1.1×10^{-4} S cm^{-1} at 30 °C [73].

A synergistic coupling effect between $Li_{6.75}La_3Zr_{1.75}Ta_{0.25}O_{12}$ (LLZTO) and poly (vinylidene fluoride) (PVDF) in the presence of N,N-Dimethylformamide (DMF) has been reported, which induced high ionic conductivity of about 5×10^{-4} S cm^{-1} at 25 °C, satisfactory mechanical strength, and good thermal stability of the PVDF/LLZTO composite electrolyte [74]. In this composite electrolyte, LLZTO acted as both initiator and Li^+ ion conductive filler. Meanwhile, the compling of La atoms in LLZTO with the N atoms and C═O groups of the DMF solvent molecules led to partial dehydrofluorination which thus enhanced the interactions between the PVDF matrix, lithium salt, and LLZTO particles, and significantly affected ion migration behavior in the composite electrolyte.

Very recently, Cui et al. used AlF_3 surface-modified anodized aluminum oxide (AAO) as the ceramic scaffold and poly (ethylene oxide) as the polymer matrix to construct a AAO/PEO composite electrolyte with densely packed, vertically aligned, and continuous nanoscale ceramic/polymer interfaces, giving an ionic conductivity of 5.82×10^{-4} S cm^{-1} at room temperature (Fig. 2e) [75]. This work demonstrated the importance of both interfacial chemical modification and vertically aligned continuous ceramic/polymer interfaces for maximizing the interfacial effects on enhancing ionic conductivity of composite solid-state electrolytes.

3.2. Li^+ ion transference number

The Li^+ ion transference number (t_{Li+}) can be considered as the fraction of the total ionic conductivity that is contributed by Li^+ ion. High t_{Li+} can effectively decrease the concentration polarization caused by anions accumulation especially under high C-rates. Therefore, developing high t_{Li+} solid-state electrolytes, in which the ionic current is carried predominantly by the Li^+ ion rather than its counter-ion, is of great significance to improve energy density and charging rates of batteries. Several representative strategies are listed below to review the progress in this aspect.

3.2.1. Selectively transferring Li^+ ion

The architecture design with the function of selectively transferring Li^+ ion could endow the composite electrolyte with high Li^+ ion transference number. It has been reported that the designed poly (ethylene carbonate) (PEC)/lithium montmorillonite (LiMNT) composite solid-state electrolytes with a high t_{Li+} of 0.83 by inserting PEC to the LiMNT interlayer. The high t_{Li+} was not only attributed to the amorphous PEC matrix, but also due to the selective immobilization of charged ions in the intercalated PEC/LiMNT composite electrolyte. As shown in Fig. 3a, the 2D LiMNT provides abundant Lewis acid centers to immobilize the electrolyte anions by Lewis acid-base interaction to promote the dissociation of lithium salt and release more Li^+ ion for conduction, while the carbonate groups of PEC promote the transfer of Li^+ ion selectively and quickly in intercalation space by weak interactions between carbonate groups/Li^+ ion [76].

Porous network structures with charged backbone, such as ionic covalent organic frameworks (ICOFs), are also promising alternatives as solid-state electrolytes (Fig. 3b). In ICOFs, negatively charged functional groups can be immobilized into the framework backbones to shield anions and allow solely the Li^+ ion mobility, contributing to high Li^+ ion transference number [77–80]. Zhang et al. designed and synthesized a series of single-ion conducting imidazolate ICOFs, which exhibited a high t_{Li+} of 0.81 as well as excellent room temperature ionic conductivity up to 7.2×10^{-3} S cm^{-1} due to the weak Li^+ ion/imidazolate anion binding interactions and well-defined porous 2D framework structures of ICOFs (Fig. 3c) [79].

Polymer/ceramic/polymer layered electrolyte with sandwich structure is also a typical kind of composite solid-state electrolytes, which can provide high Li^+ ion transference number. In this architecture, the introduction of the ceramic layer can block the anion transport, and the

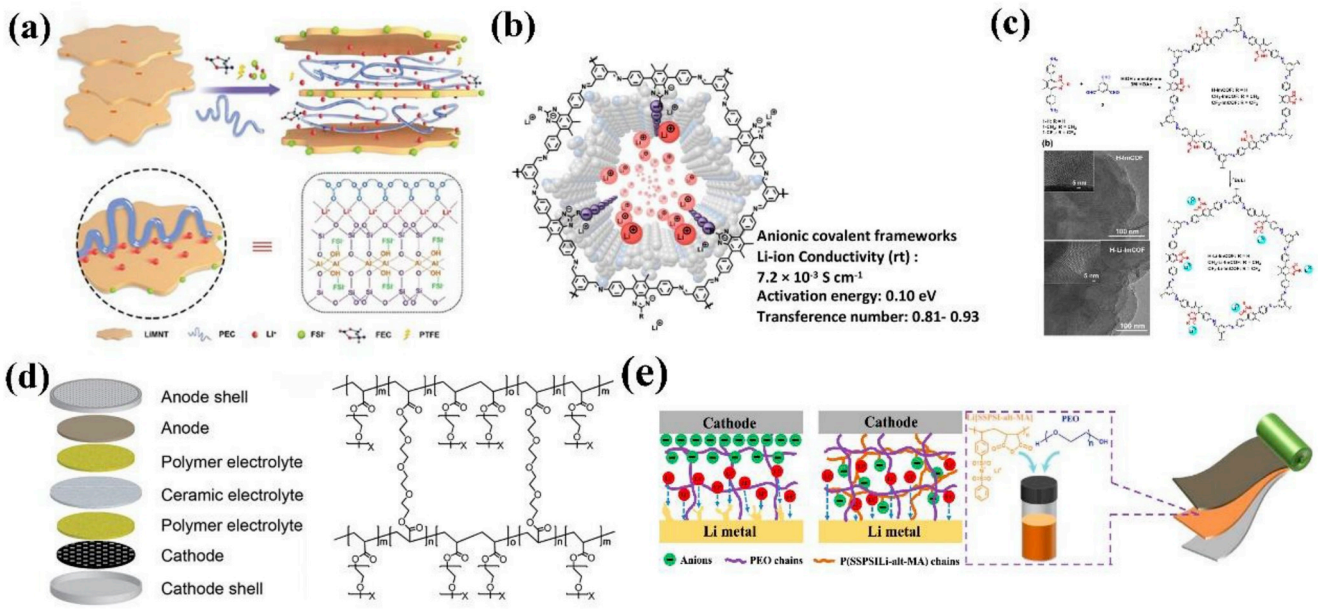

Fig. 3. (a) Schematic showing the mechanism of intercalated PEC-LiMNT with enhanced Li^+ ion transference number (Reproduced with permission [76]). Mechanism of Li^+ ion transfer in Li-ImCOFs; (c) TEM images and synthesis route of Li-ImCOFs (Reproduced with permission [79]). (d) Sandwich structured solid-state battery and molecular structure of polymer layer (Reproduced with permission [81]). (e) Schematic mechanism of solid-state electrolytes with high Li^+ ion transference number inhibiting lithium dendrites and the molecular structure of the single-ion composite polymer electrolyte (Reproduced with permission [84]).

polymer layer possesses better wetting ability toward electrodes [81–83]. Goodenough et al. prepared a sandwich composite electrolyte using cross-linked polyethylene glycol methyl ether acrylate (CPMEA) polymer electrolyte and LATP ceramic pellet sandwiched within the polymer electrolyte, which integrated the advantages of polymer and ceramic pellet, achieving a high t_{Li+} number of 0.89 and favorable interfacial properties (Fig. 3d) [81].

3.2.2. Using single ion conducting polymer lithium salts

Single-ion-conducting polymers have attracted more and more attention to be a component in the composite electrolytes to enhance Li^+ ion transference number. In this kind of electrolytes, a lithium salt with anion covalently attached to the polymer backbones is utilized. In this case, the anions are immobilized, only the transport of Li^+ ion can take place, featuring high t_{Li+} near unity [37–39,84–87]. Feng et al. prepared a single-ion conductive polymer with an alternating structure of maleic anhydride (MA) and lithium 4-styrenesulfonyl (phenylsulfonyl)imide, which was mixed with PEO to obtain a composite electrolyte with high room temperature ionic conductivity up to 3.08×10^{-4} S cm^{-1} and extremely high t_{Li+} up to 0.97 (Fig. 3e) [84]. This composite electrolyte exhibited the ability to hinder the formation and growth of lithium dendrites due to high t_{Li+}, which suppressed the concentration gradient near the anode, and therefore lowered the driving force for dendrite formation.

Fig. 4 summarizes the distribution of composite solid-state electrolytes in the ionic conductivity-Li^+ ion transference number 2D plots [59,69,76,79,84,88–103]. It can be observed that no matter the continuous phase is PEO or polyester, the ionic conductivity can be improved more than 10^{-4} Scm^{-1} at room temperature by introducing the second phase (polymer or inorganic materials) to decrease the crystallinity of the continuous phase. The faster Li^+ ion transport channel can be constructed by continuous and ordered structure of fillers. Compared with PEO, polycarbonates, like PPC and PEC are more favorable for high Li^+ ion transference number. Especially, the single-ion conductor can reach a Li^+ ion transference number to a value higher than 0.8.

3.3. Anode/electrolyte interface

Lithium metal is the "holy grail" of anode materials due to high energy density, but its extremely high activity in liquid electrolyte systems leads to big safety risks [14]. Replacing liquid electrolytes with solid-state electrolytes provides a promising opportunity to tackle the safety issue of lithium anodes. However, the subsequent interface problems, such as poor wettability between lithium anode and solid-state electrolytes, side reactions, lithium dendrite-formation and the contact failure induced by volume change of lithium anode, still exist and limit the development of solid-state batteries with lithium metal anode [104]. Several representative strategies are listed below to review the efforts that have been made to address the interfacial issues between lithium anode and composite solid-state electrolytes.

3.3.1. Designing rational interfacial layer

Flexible interfacial layers such as organic polymers [83,105–107], gels [108,109] and ionic liquids (ILs) [110,111] are able to change the rigid contact between solid-state electrolytes and lithium metal electrode to soft contact, which can not only reduce the interface impedance of lithium metal/solid-state electrolytes to facilitate the rapid transfer of Li^+ ion at the phase interface, but also can favor the uniform deposition of lithium to inhibit the growth of lithium dendrite. Ding et al. proposed a simple method of suppressing lithium dendrites by using PEO interfacial layer between LAGP-PEO composite solid-state electrolytes and lithium anode [19]. The presence of PEO layer on lithium anode not only resulted in satisfactory interface contact, but also prevented lithium anode from reacting with LAGP.

Furthermore, the PEO interfacial layer synergistically contributes to the inhibition of lithium dendrite by combining with composite solid electrolyte. Li et al. reported a dendrites resistant and ionic conductive 3D cross-linked gel polymer electrolyte layer at the interface between LAGP pellets and lithium metal, which not only avoided side reactions between LAGP pellets and lithium metal anodes, but also reduced the interfacial impedance from 20 kΩ to 460 Ω (Fig. 5a) [109]. Moreover, the soft 3D layer could act as a buffer to relieve the stress generated by the volume change of lithium anodes during cycling. The unique properties of 3D gel layer guaranteed the stable cycling and impressive

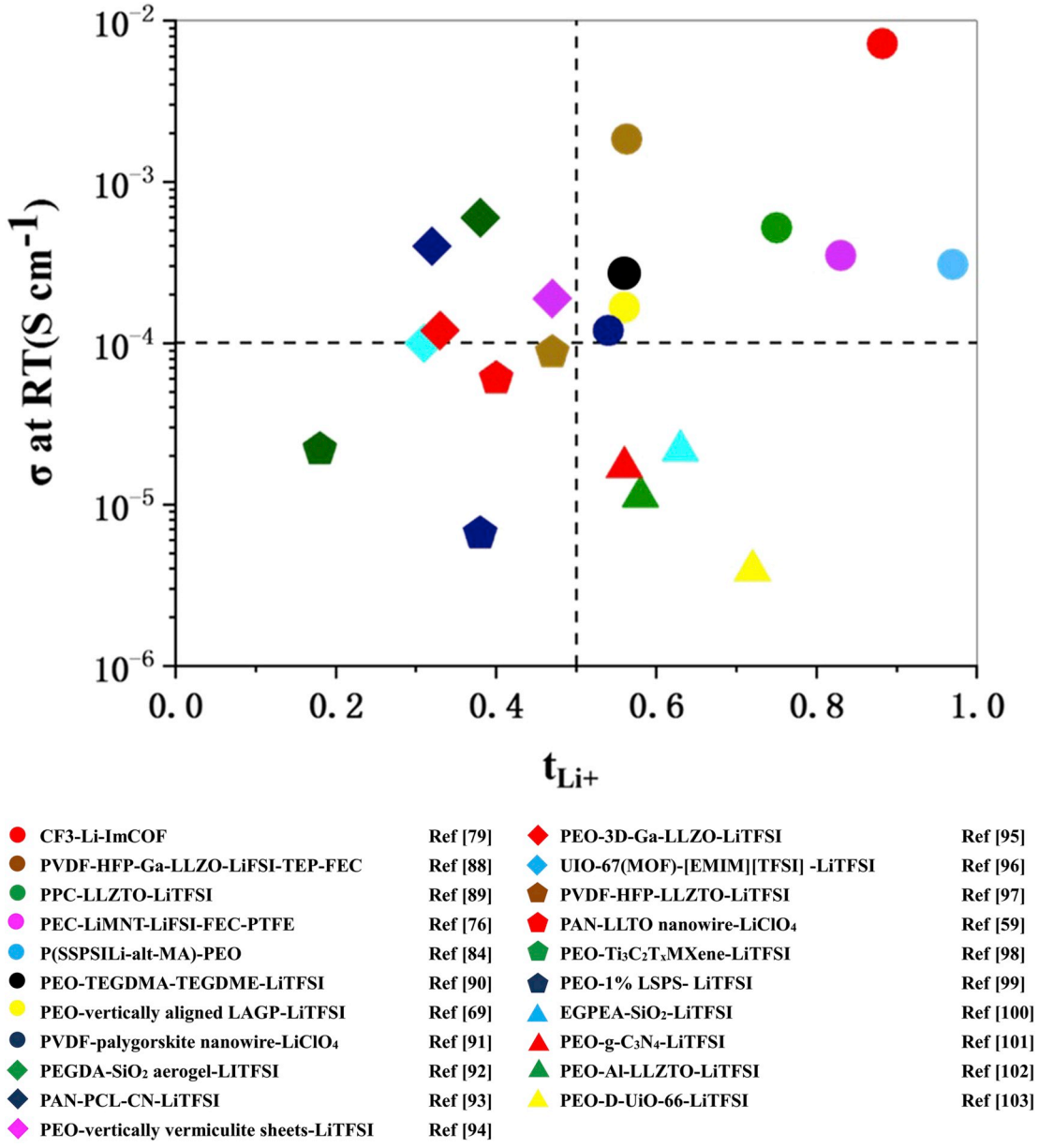

Fig. 4. A summary of the room-temperature ionic conductivity and Li^+ ion transference number of recent composite solid-state electrolytes.

capacity retention of 91.2% of $LiFePO_4$ (LFP)-based lithium metal batteries at room temperature for 300 cycles. Guo et al. designed a viscoelastic and non-flammable interface with ILs, which not only ensured the intimate and uniform contact between composite solid electrolyte and electrode to decrease interface impedance and avoids the contact loss during cycling, but also enabled the construction of fast Li^+ ion transport pathway between composite solid electrolyte and electrode to improve the kinetic process (Fig. 5b) [111]. Benefiting from this novel design, solid lithium metal batteries with both $LiFePO_4$ and $LiCoO_2$ as cathodes exhibited excellent cycling and rate performance, such as a discharge capacity of 157mAh g^{-1} after 100 cycles at C/2 and 97mAh g^{-1} at 5C for $LiFePO_4$ cathode. In addition, the lithium anode exhibited a smooth and uniform surface after long-term cycling which means that the dendrite was successfully inhibited.

The design of interfacial layer between lithium metal and solid-state electrolytes should also take into account the ion transport performance. The interfacial layer with high Li^+ ion transference number can provide larger amount of available uniform Li^+ ion flux to enhance the uniformity of lithium deposition at the interface, and improve the Coulombic efficiency of the battery [112–116]. Goodenough et al. used a single ionic conductor polymer wetting layer to coat on the LLZTO pellet to obtain an inorganic-organic composite solid-state electrolytes [106]. The superior adhesion with lithium electrode and high Li^+ ion transference number of interfacial layer favored a uniform lithium deposition to achieve dendrite-free lithium anode. The solid-state $LiFeO_4$/Li battery using this electrolyte achieved the first Coulombic efficiency up to 97%, and a notably high Coulombic efficiency of 99.9–100% after 160 cycles at 0.2C.

3.3.2. *In situ polymerization*

Designing the integrated interface between solid-state electrodes and solid-state electrolytes by in situ polymerization is a representative strategy to improve the interface issues between them [117–121]. Cui et al. injected the liquid monomers with lithium salt into the cell and then initiated the in situ formation of poly (vinyl carbonate) (PVCA)--LiSnPS composite solid-state electrolytes on the electrode by thermal polymerization (Fig. 5c) [118]. This process engineered an integrated solid-state electrodes/electrolyte interface with an efficient Li^+ ion

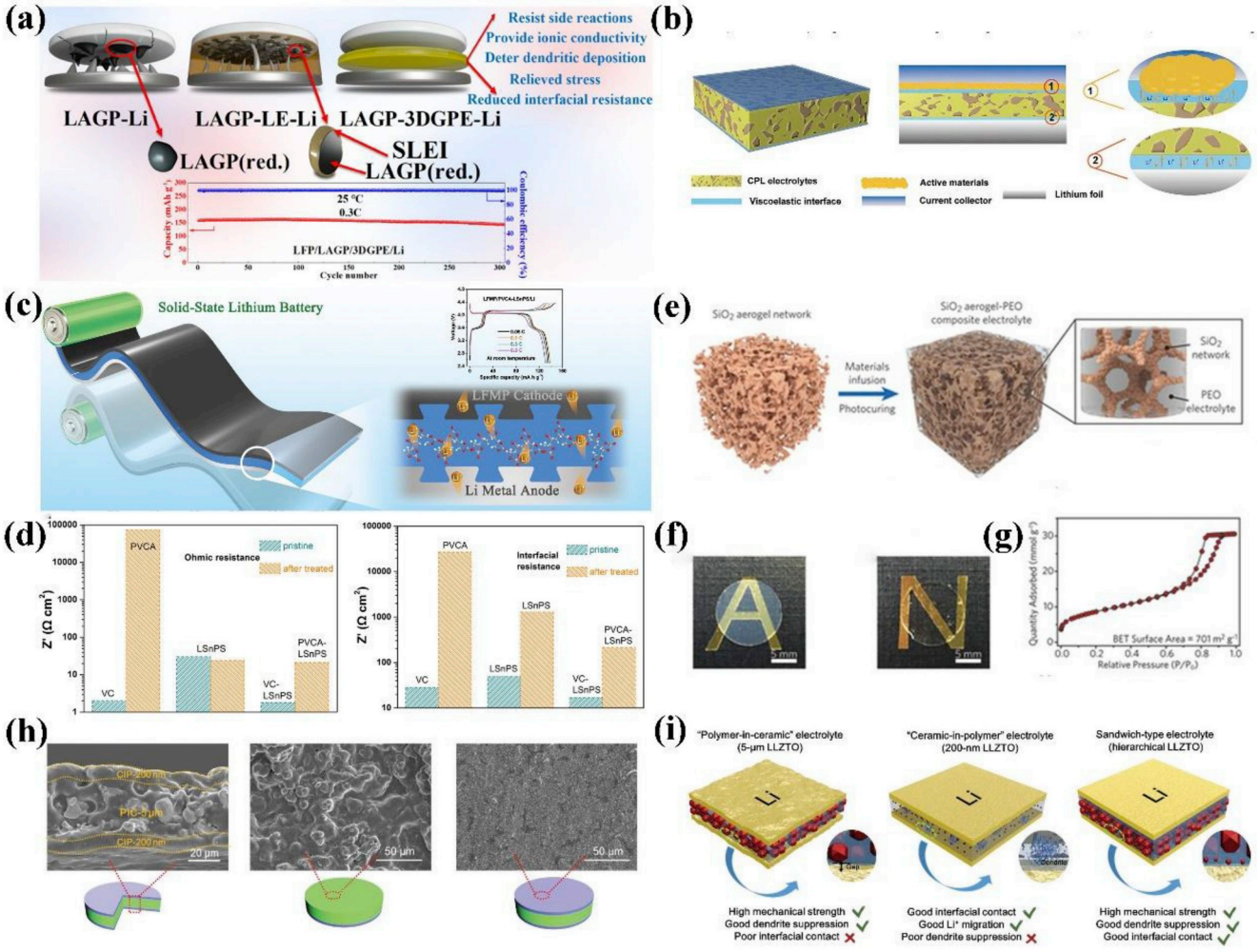

Fig. 5. (a) Protection mechanism with different electrolyte systems and cycling performance of LFP/LAGP/3DGPE/Li cell at 0.3C (Reproduced with permission [109]). (b) Design for viscoelastic IL interface layer contacting behavior with anode/cathode (Reproduced with permission [111]). (c) Schematic solid-state battery constructed by in situ polymerization and (d) Ohmic/interfacial resistance between various electrolytes and lithium metal in Li–Li symmetrical cells (Reproduced with permission [118]). (e) The synthetic procedures of SiO_2-aerogel-reinforced solid-state electrolyte; and (f) digital photo images of ceramic-polymer composite solid-state electrolytes; (g) BET surface area of SiO_2-aerogel (Reproduced with permission [92]). (h) The cross-sectional/top-view SEM images of composite solid-state electrolytes with hierarchical structure; (i) The wettability and lithium dendrite growth of electrodes with different structures (Reproduced with permission [131]).

transport pathway to significantly decrease the interfacial resistance from 1292 to 213 Ω cm^2 (Fig. 5d). In their later work, a 3D crosslinked composite solid electrolyte was in situ formed on the surface of lithium metal by copolymerized vinylene Carbonate (VC) and methacryloxy propyl trimethoxyl silane (KH570)-modified LLZO fast ion conductor [117]. The coordination interaction of –O(C═O)O- functional groups of the polymer with Li^+ ion favored the uniform deposition of lithium, and high mechanical strength provided by LLZO particles could block the dendrite growth. The composite solid-state electrolytes was used to assemble battery with $LiNi_{0.5}Mn_{1.5}O_4$ cathode and lithium metal anode, which presented significantly reduced interfacial resistance and excellent capacity retention.

3.3.3. *Adopting high modulus electrolytes*

High mechanical modulus composite electrolytes can act as physical barrier to mechanically inhibit the formation of lithium dendrites [60,97,122]. Generally speaking, the introduction of inorganic fillers in composite solid-state electrolytes would provide enhanced hardness to resist the formation and growth of lithium dendrites [15,44,123]. For example, the modulus of composite solid-state electrolytes could be reinforced to 0.43 GPa by introducing mesoporous SiO_2 aerogel into poly (ethylene glycol)diacrylate (PEGDA) (Fig. 5e and f) [92]. The connected SiO_2 aerogel not only served as a strong pillar to effectively suppress lithium dendrite growth, allowing a prolonged cycling without short circuit, but also provided a large and continuous surface for strong anion adsorption, resulting in a high ion conductivity of 0.6 mS cm^{-1} (Fig. 5g). The $LiFePO_4$/Li full cell with this composite solid-state electrolytes exhibited superior cycle and rate performances at room temperature and high cathode capacity up to 2.1mAh cm^{-2}.

In addition to rigid inorganic particles, engineering the rigid composite skeleton is also an effective strategy to increase the mechanical strength of composite solid-state electrolytes [124,125]. Fan et al. reported a 3D LATP/PAN fiber-network-reinforced PEO-based composite solid electrolyte for dendrite-free lithium anode [126]. This architecture helped to enhance the electrochemical stability of electrodes/electrolyte interface by isolating lithium anode from LATP and suppress lithium dendrite growth by the mechanical reinforcement of fiber network, leading to a long-term stability and safety of the Li/Li symmetric battery under a current density of 0.3 mA cm^{-2} for 400 h without short circuit.

High mechanical strength of solid-state electrolytes may lead to contact problems with the electrodes, therefore it is important to reach a compromise between the mechanical strength and flexibility to

simultaneously achieve lithium dendrites suppression and low interfacial resistance [44,127–130]. Sun et al. fabricated different composite electrolytes from "polymer in ceramic" (PIC) to "ceramic in polymer" (CIP) by using different LLZTO concentrations and particle sizes [131]. As shown in Fig. 5h, the CIP with 20 vol% 200 nm LLZTO particles shows good flexibility and high ionic conductivity, while the PIC with 80 vol% 5 μm LLZTO particles exhibits excellent tensile strength. A sandwich-type composite solid-state electrolytes was rationally designed with a mechanically strong PIC interlayer to suppress lithium dendrite by physical obstacles and flexible CIP outer layers to allow good interfacial contact. Such composite electrolyte with hierarchical LLZTO particles successfully achieved both dendrite suppression and excellent interfacial contact with electrodes (Fig. 5i). The solid-state Li/Li symmetrical cells and the LFP/Li full cells using this composite electrolyte demonstrated excellent electrochemical performance at room temperature.

3.3.4. Using self-healing polymers

The self-healing materials possess good viscoelasticity to better accommodate the volume change of electrodes and enhance the wettability of electrodes. Meanwhile, the self-bonding property of self-healing polymer can avoid the crack-induced contact failure during cycling. The uniqueness of self-healing materials has driven great advances in deformable and reconfigurable electronic devices [132–134].

Whiteley et al. firstly reported the preparation of ultrathin composite electrolyte membranes (64 μm) by mixing self-healing polyimine and Li_2S–P_2S_5 powder under hot-press for battery with lithium anode, which demonstrated good performance [132]. Later, using self-healing polymer to stabilize lithium anodes has attracted more and more attention. Liu et al. fabricated a composite electrolyte consisting of self-healing polymer and LLZGO nanoparticles, which provided strong adhesion with lithium anode, good accommodation to volume change of lithium anode, and seal-healing functionality to avoid crack-induced battery failure during cycling (Fig. 6a) [134]. Benefiting from these advantages of composite electrolyte, the Li/Li symmetric cells exhibited uniform lithium deposition and the smallest polarization of 240 mV to date over 1500 cycles even at ultra-high current density up to 20 mA cm^{-2} (Fig. 6b). The Li/$Li_4Ti_5O_{12}$ cells based on this electrolyte achieved a stable cycling for 120 cycles at 0.2C with a high specific capacity of 157 mAh g^{-1} and a capacity retention of 99.4%.

3.3.5. Using elastic electrolytes

Elastomers have the ability to recover from the applied stress with high toughness and repeatability. The elastic electrolyte can provide good interfacial contact with the electrodes even when large volume change occurs during cycling, and meanwhile, an electrolyte with high resilience would protect the batteries against external impacts (Fig. 6c) [135–138]. These characteristics of elastomer makes it an ideal choice for solid-state electrolytes. Cui et al. designed a composite solid-state electrolytes by blending poly (propylene oxide) (PPO) elastomer, SiO_2 nanoparticles, LiTFSI, and liquid plasticizer propylene carbonate (PC), which demonstrated a high mechanical resilience (0.32 MJ m^{-3}) and a high ionic conductivity of 0.25 mS cm^{-1} at room temperature (Fig. 6d) [135]. Using this elastic electrolyte, the solid $LiFePO_4$/Li battery cycled for 300 cycles with a high cathode capacity of 152 mAh g^{-1} at room temperature. As shown in Fig. 6e, the pouch cell assembled with this electrolyte can maintain stable potential even after intense mechanical impact testing.

3.4. Cathode/electrolyte interface

Currently, the cathode materials are being continuously developed towards higher capacity and higher voltage. Although the solid-state electrolytes have better tolerance with high voltage cathode materials

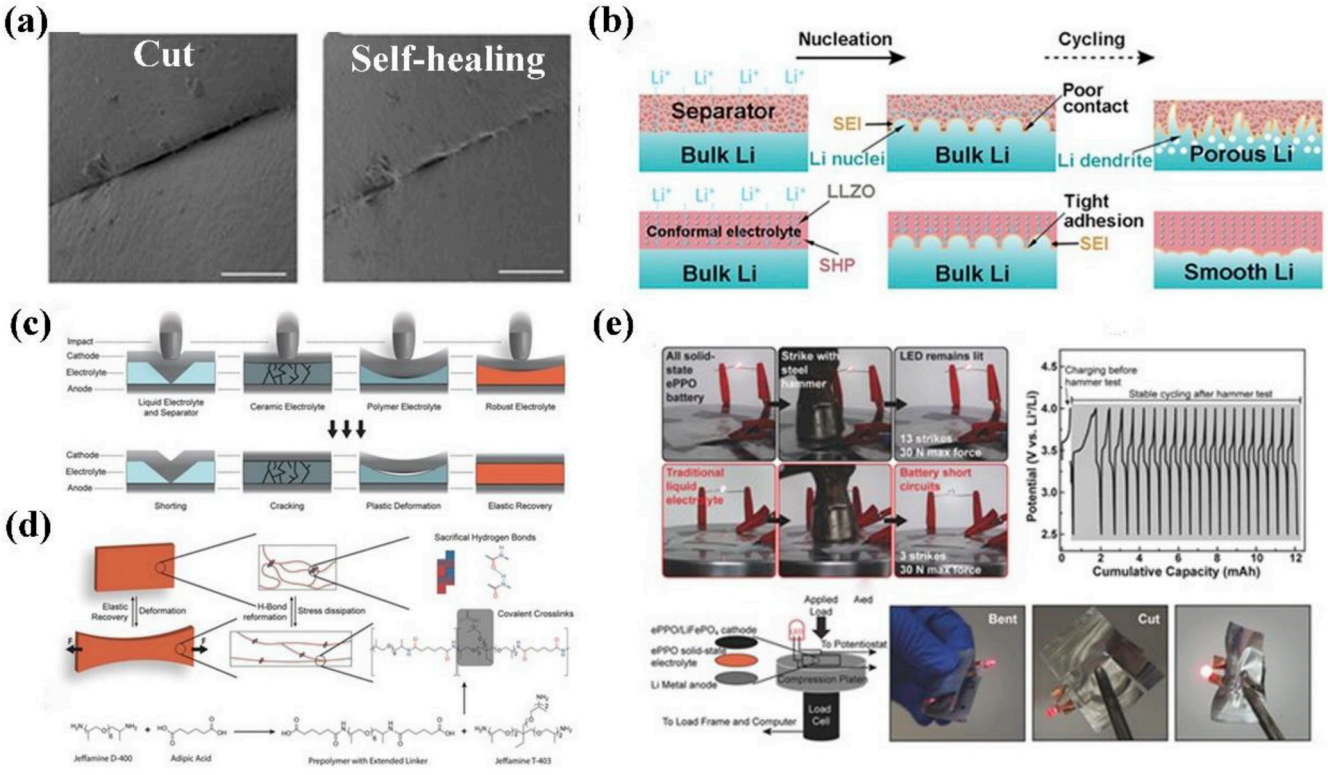

Fig. 6. (a) SEM image of composite solid-state electrolytes with self-healing performance; (b) Multifunctional composite solid-state electrolytes with self-healing property showing stable electrochemical stripping/plating behavior on lithium metal compared with the traditional separator (Reproduced with permission [134]). (c, d) Conceptual design, fabrication procedures, and chemical structure of elastomer; (e) Photographs of punch cells with composite solid-state electrolytes and liquid electrolyte undergoing hammer impact tests (Reproduced with permission [135]).

than liquid electrolytes, the cathode/solid-state electrolytes interface problems such as large interfacial impedance, interfacial element interdiffusion, interfacial side reaction caused by high-voltage decomposition and space charge layer still remain big obstacles for the practical application of solid-state lithium batteries [139,140]. Most works focus on the structure modification of cathode materials to address the above-mentioned problems [141–144]. In this section, we have summarized the current progress in addressing the cathode/electrolyte interfacial issues by the structure design of solid-state electrolytes.

3.4.1. Integrated cathode/solid-state electrolyte structure

The interfacial contact between cathode/electrolyte in traditional liquid lithium ion batteries and solid-state lithium batteries is quite different. The liquid electrolytes can wet the cathode well, while the cathode/solid-state electrolytes is in rigid contact, leading to large interfacial resistances [46,145].

The most commonly used strategy for decreasing interfacial resistance is to add the components of composite solid-state electrolytes (polymer and lithium salt) into cathode active materials or replace the traditional binder with polymer components in composite electrolyte [146–149].

In addition, the integrated cathode/solid-state electrolytes structure is also effective to decrease the interfacial resistance between them. One way is to make the solid-state electrolytes component permeate into the cathode active materials by heating, casting or in situ polymerization [121,150,151]. He et al. applied PEO as both the binder of cathode and the organic component of composite solid-state electrolytes [150]. The PEO in both cathode and solid-state electrolytes was fused under heating to form an integrated structure as confirmed by SEM shown in Fig. 7a, which can effectively strengthen the interface compatibility between cathode and composite solid-state electrolytes, as well as accommodate the volume change of cathode during charge/discharge cycling. The Li/Li symmetric cells using this composite solid electrolyte kept stable cycling for 1000 h without short circuit at 60 °C, and the integrated $LiFePO_4$/Li batteries also showed excellent cycling stability. Wang et al. directly casted the PEO-based electrolyte on cathode to enhance the wetting of solid-state electrolytes with the cathode and reinforce the interfacial adhesion between them (Fig. 7b) [151]. The cathode-supported solid electrolyte membrane was directly combined with a metal lithium anode to assemble solid-state $LiFePO_4$/Li cells, which exhibited reduced overall impedance by an order of magnitude and superior battery performances than conventional solid-state lithium ion batteries employing separate solid-state electrolytes membrane.

Another way is to design porous solid-state electrolytes as a host for the loading of cathode materials [128,152,153]. Hu et al. designed a 3D bilayer solid-state electrolytes framework with a thick porous garnet layer to mechanically support the thin dense garnet layer [152]. As shown in Fig. 7c, the porous layer serves as a host to load the cathode materials and provides continuous ion transport pathways, which can ensure superior cathode/solid-state electrolytes interfacial contact, and accommodate the volume change of cathode. The thin dense bottom layer is a rigid barrier with high elastic modulus to efficiently prevent lithium dendrite penetration. Such structure allowed high sulfur cathode loading, and the S/Li battery exhibited high energy density and high initial and average Coulombic efficiency up to 99%.

How to achieve the seamless atomic-level contact solid-solid cathode/electrolyte interface comparable to solid-liquid contact is a notable direction. Very recently, Nan et al. embedded the Li-rich layered electrode into the LLTO lattice, and the epitaxial interface between the electrode material and the solid-state electrolytes is formed due to the periodic misfit between the perovskite electrolytes and the layered electrode, thus fabricating a solid-solid interface with efficient Li^+ ion transfer ability. Although this mechanism is expected to apply to perovskite materials, it provides a new strategy for achieving excellent cathode/electrolyte interfaces [154].

3.4.2. Using high-voltage resistant electrolytes

Currently, although many works have reported solid-state electrolytes with an electrochemical stability up to 4.4V, which is higher than the operating voltage of LFP, most solid-state batteries are still LFP-based [19,101,155–157]. The crosslinking between different organic or inorganic components has been demonstrated to be an effective method to extend the electrochemical window of PEO-based electrolytes [90,124,158–160]. Liu et al. prepared a flexible PEO-based composite solid-state polymer electrolyte through UV-induced in situ polymerization of PEO, tetraethylene glycol dimethacrylate (TEGDMA) and

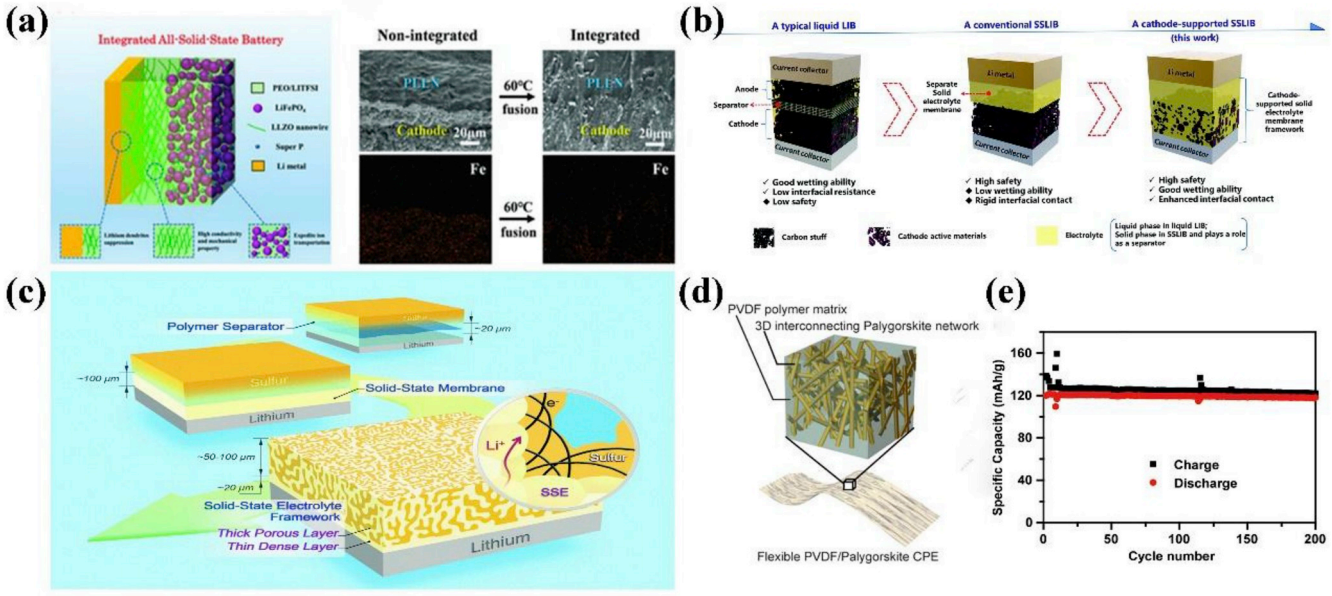

Fig. 7. (a) Schematic diagram of integrated solid-state LFP/Li battery, SEM images and EDS images of cross-section (Reproduced with permission [150]). (b) Structure of the cathode-supported solid-state battery (Reproduced with permission [151]). (c) The 3D bilayer solid-state electrolytes framework for integrated solid-state S/Li battery (Reproduced with permission [152]). (e) Schematic illustration of 3D structure of the flexible PVDF/palygorskite nanowire composite solid-state electrolytes. (f) Cycling performance of solid-state LCO/Li battery (Reproduced with permission [91]).

tetraglyme (TEGDME), which exhibited an outstanding electrochemical window up to 5.38 V vs. Li^+/Li [90]. Xie et al. prepared a flexible organic-inorganic composite solid-state electrolytes via thiol-acrylate photopolymerization of thiol-modified silica nanoparticles and poly (ethylene glycol) diacrylate under UV irradiation, which demonstrated a high electrochemical window of 5.0 V vs Li^+/Li, and the LFP/Li solid-state battery exhibited a stable cycling under the extended voltage range of 2.5–4.3 V [159]. Wan et al. developed a composite solid-state polymer electrolyte with rigid-flexible structured interpenetrating poly (ether−acrylate) (ipn-PEA) network by photo-polymerization of ion conductive PEO and branched acrylate, which was paired with cathodes with a working potential within 4.5 V vs Li^+/Li to enable a powerful cell that can effectively operate at 5 C and cycle stably at 1 C at room temperature [124].

Clearly, exploring high-voltage resistant solid-state electrolytes is of great importance for the application of cathode materials with higher capacity and voltage such as $LiNi_xMn_yCo_zO_2$ (NMC) in high-energy-density lithium batteries. Using polymers that are resistant towards oxidation such as PAN [59,161], PVDF [74,91,162,163], PVDF-HFP [164] can also enhance the high-voltage resistant properties of composite electrolytes. Yang et al. used high-voltage resistant PVDF as polymer matrix and palygorskite nanowire ($(Mg,Al)_2Si_4O_{10}(OH)$) as ceramic filler to prepare a composite electrolyte, which can be paired with the cathode material $Li(Ni_{1/3}Mn_{1/3}Co_{1/3})O_2$ (NMC111) to present a high capacity of 121.4 mAh g^{-1} and a high capacity retention of 97% after stably cycling for 200 cycles at C/3 [91]. Wen et al. prepared a PVDF-HFP based composite electrolyte by in situ crosslinking of PVDF-HFP with $Li_{6.4}Ga_{0.2}La_3Zr_2O_{12}$ (Ga-doped LLZO) as initiator and ion conductive filler, which demonstrated a wide electrochemical stable window of 4.75V, and can be paired with NCM523 cathode to exhibit improved cycling stability at 0.5C [165].

3.4.3. Engineering Janus interfaces of composite solid-state electrolytes

Solid-state electrolytes that are simultaneously compatible with high-voltage cathode and lithium metal anode are promising candidates for solid-state batteries with high-energy density [17,166]. The asymmetrical design of solid-state electrolytes has been proposed to be an effective method to satisfy the different demands of anode and cathode (Fig. 8a) [167–170]. Guo et al. constructed an asymmetric ultrathin (7.5 μm) composite solid-state electrolytes with PEGMEA soft polymer layer in situ contacting with cathode to reduce interface resistance, and PEO/LLZO rigid layer contacting with lithium anode to inhibit lithium dendrite [167]. The solid-state $LiFePO_4$/Li battery assembled with this Janus electrolyte possessed a capacity retention of 94.5% over 120 cycles and a Coulombic efficiency exceeding 99.8%. Goodenough et al. synthesized a new high-voltage resistant poly (N-methylmalonamide) (PMA) polymer electrolyte by polymerizing dimethylacetamide (DMAc) with high dielectric constant (Fig. 8b). After that, a double-layer PEO/PMA polymer composite solid electrolyte was prepared, in which PEO was in contact with lithium anode to favor the lithium dendrite-free plating, and PMA allowed the Li^+ ion extraction from $LiCoO_2$ cathode without the electrolyte oxidation at 4 V [168].

Guo et al. fabricated a Janus PAN@LAGP composite electrolyte with PAN enrichment on one side and LAGP on the other side as intermediate layers, which was coupled with an oxidation-resistant PAN layer and reduction-resistant PEGDA layer to get a heterogeneous multilayered composite solid electrolyte [169]. As shown in Fig. 8d, the PAN-rich side contacts with the PAN layer on the cathode for good cathode/electrolyte interface compatibility, while the LAGP-rich side contacts with the PEGDA layer on the anode to avoid side reaction between LAGP and lithium anode. Moreover, this electrolyte exhibited broaden electrochemical window of 0–5 V. By pairing with $LiNi_{0.6}Co_{0.2}Mn_{0.2}O_2$ and $LiNi_{0.8}Co_{0.1}Mn_{0.1}O_2$ cathodes, the solid-state lithium metal batteries

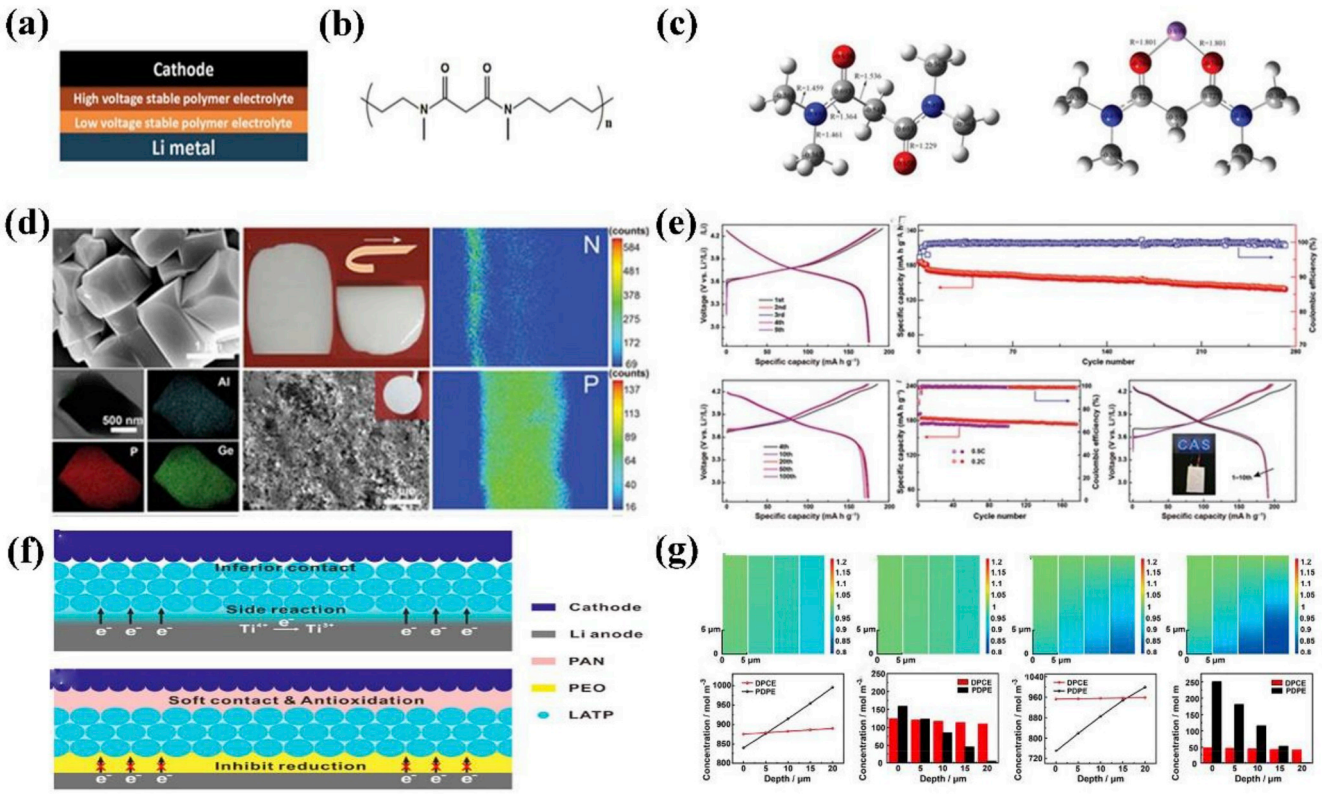

Fig. 8. (a) Model of solid-state battery with a double-layer electrolyte. (b) Molecular structure of high-voltage resistant polymer electrolytes. (c) Simulations of a simplified fragment of PMA with Li^+ ion coordination (Reproduced with permission [168]). (d) SEM image and the EPMA-EDS diagrams of composite solid-state electrolytes with a Janus and flexible structure. (e) Typical charge/discharge profiles and cycling stability of solid-state NCM/Li battery (Reproduced with permission [169]). (f) Illustrations of engineering Janus interfaces and (g) COMSOL simulation results of ion concentration ascending along the lithium anode interface (Reproduced with permission [170]).

exhibited high capacity, good cycling stability and effective inhibition of dendrite formation (Fig. 8e). In their later work [170], they introduced oxidation-resistant PAN and reduction-resistant PEO to the opposite sides of LATP pellets to get composite solid-state electrolytes with Janus interfaces (Fig. 8f). COMSOL simulation demonstrated that ions were uniformly distributed across the interface due to the inorganic LATP layer (Fig. 8g). The construction of stable electrode/solid electrolyte Janus interfaces endowed the LATP ceramic pellets with integrated functions of superior wetting ability with high-voltage cathode and suppressing lithium dendrite growth.

3.5. Performance of solid-state batteries

The aim to develop solid-state electrolytes is to increase the safety and energy density of batteries. The batteries integrating PEO electrolyte with LFP cathode and lithium anode have already been commercially used in the Bolloré Bluecar [41]. The composite solid-state electrolytes are designed to combine the advantages of polymer and inorganic electrolytes. However, the development of composite solid-state batteries is still facing practical challenges.

As shown in Table 1, although numerous composite solid-state electrolytes show wide electrochemical window ($\geq$4.7V), there are only limited reports about batteries working with high-voltage cathode (NCM811, NCM622 etc.). The measurement results of electrochemical window seem not completely consistent with the stability of composite solid-state electrolytes in batteries. The organic parts are usually the short boards of the composite systems. The PVDF-based and PAN-based composite solid-state electrolytes match better with high-voltage cathodes than polyether-based composite solid-state electrolytes. It is worth noting that although PEO polymer matrix is prone to decompose at high-voltage, PEO-based solid-state batteries coupled with high-voltage cathode have also been reported [103]. This interesting result demonstrated that the inorganic ingredients play an important role in the stability of composite solid-state electrolytes in batteries. Therefore, exploring the stability mechanism of composite solid-state electrolytes at high voltage is a topic worthy of research.

A particular issue for solid-state batteries is how to form an efficient cathode/solid-state electrolyte interface that enables the battery to achieve the entire electrode capacity. Compared to a liquid-electrolyte battery, where the electrolyte spontaneously permeates through the pores of the electrode to wet the active material surface, in a solid-electrolyte system the capacity needs to be ascertained by adding a certain amount of electrolyte into the cathode.

Compared with batteries using liquid electrolyte, the mess loading of active material is still lower in solid-state batteries. In addition, the thickness of solid-state electrolytes layer is usually high. How to decrease the concentration of inactive component in the solid-state batteries without sacrificing performance is still a challenge for improving energy density.

Most importantly, solid-state batteries are still often only operational at high temperatures (50–80 °C), because high Li^+ ionic conductivity and electrodes/electrolyte interface will only be sufficient at these high temperatures. Therefore, developing solid-state batteries that can be operated at room temperature or even in extreme conditions is also an attractive topic.

3.6. Advanced computational simulations and characterization in solid-state LIBs

Advanced computational simulation and characterization techniques can provide in-depth understanding of ions transport mechanisms and electrodes/electrolyte interfacial electrochemical processes, and therefore play an important role in guiding the structural design of composite solid-state electrolytes material.

Although many characterizations such as X-ray techniques and image techniques have been developed based on traditional liquid electrolytes-based LIBs, they are inapplicable for the solid-state lithium batteries and unable to directly obtain the real-time information about the solid-solid interface in working condition. To develop new advanced computation simulations and nondestructive in situ and operando techniques are very necessary for us to real-time monitor and analyze the complex interface processes, as well as the Li^+ ion transport at both solid-solid electrolyte components interface and electrodes/electrolyte interface. In recent years, great efforts have been made to explore advanced microstructure and chemical composition analysis, and the electrochemical analysis techniques applicable for the solid-state batteries interface.

3.6.1. Advanced computational simulations

Molecular dynamics (MD) simulation like first-principle MD simulations or ab initio MD simulations relies on Newtonian dynamics to simulate the motion of the molecular, and can capture the ions diffusion in the battery materials in real-time [173,174]. The dynamics of ions can be directly observed by MD simulation to determine the details of diffusion mechanism, such as ion pathway and ion diffusion by modeling the real-time dynamics of all ions in the material. For inorganic lithium ionic conductors with crystal structure, the first principle MD simulations can accurately simulate the diffusion behavior of lithium ion in them, which can dynamically evaluate ionic conduction mechanisms. Tse et al. calculated the diffusion coefficients of β-Li_3PS_4 and γ-Li_3PS_4 with the first principle MD, and believed that the higher conductivity of β-Li_3PS_4 comes from the intrinsic lithium vacancy, and the higher Li^+ ion mobility in the nanoclusters is due to the more defects and large surface area [175]. Later, Sicolo et al. successfully revealed the diffusion mechanism of a new sulfide superionic conductor Li_4PS_4I by using MD simulation, and calculated the diffusion coefficient and activation barrier of lithium ion [176]. In addition, ab initio MD simulations can be applied to investigate the stability of interfacial structure and phase by combining with other theories. Deng et al. rationally optimized the lithium-rich $Li_3OCl_{1-x}Br_x$ anti-perovskite superionic conductors under the guidance of first principles calculations and percolation theory [177]. Furthermore, ab initio MD simulations confirmed that the existence of potential phase in this structure, which is beneficial to lithium ion transport. Balbuena et al. used ab initio MD simulation combined with density functional theory to explore the interface stability between lithium metal and solid-state sulfide electrolytes ($Li_{10}GeP_2S_{12}$, $Li_2P_2S_6$, β-Li_3PS_4, and $Li_7P_3S_{11}$), and revealed the main interface side products between electrolytes and lithium metal in detail [178]. These methods based on molecular dynamics simulation provides strong theoretical support for understanding ion transport mechanism and interface stability.

3.6.2. Characterization on Li^+ ion transport

3.6.2.1. Neutron techniques. Neutron techniques like neutron diffraction (ND) or neutron depth profiling (NDP) mainly use the neutron stream as the incident beam to irradiate materials and collect the information about the material structure and ion distribution. Neutron techniques have a deeper detection range than ordinary X-rays and can detect the position of H and Li in the lattice because of high sensitivity of neutron to light elements [179]. In addition, the depth of neutron techniques can penetrate the whole battery to realize the simultaneous detection of cathode and anode. Based on the above advantages, neutron techniques not only accurately detect the electrodes or solid-state electrolytes structure, but also can conduct operando test on batteries. Typically, ND analysis can qualitatively determine the location and content of Li^+ ion, and thus guide the design of crystal structure. Kamaya et al. explored the structure of a new solid-state superionic conductor $Li_{10}GeP_2S_{12}$ by means of ND, which showed that the unit cell has a space group structure of $P4_2/nmc$ (137) [24]. However, the signal to noise ratio of the ND pattern will be reduced when testing H in the sample,

Table 1
Overview of lithium batteries employing composite solid-state electrolyte.

Composite solid-state electrolyte	Ionic conductivity and Li^+ ion transference number	Electrochemical window	Cathode material and mass loading	Performance	Reference
Multilayer with PAN@LAGP-LiTFSI and PEGDA-LiTFSI	3.7×10^{-4} S cm^{-1} at 25 °C	5V	7:1:1:1 NMC811/NCM622/Super P/PVDF/PAN 3–5 mg cm^{-2}	NCM622/Li: 25 °C, 0.5C, 2.8 V–4.3 V 1st discharge: 180 mA h g^{-1} at 0.1C. 270th capacity retention: 81.5%. Coulombic efficiency: 99.8% NCM811/Li: 25 °C, 0.5C, 2.8 V–4.3 V 1st discharge: 175 mA h g^{-1}. 100th discharge: 170 mAh g^{-1}. Capacity retention: 97.7%.	[169]
PVDF-5 wt% palygorskite ((Mg, Al)$_2$Si$_4$O$_{10}$(OH)) nanowires-$LiClO_4$	1.2×10^{-4} S cm^{-1} at 25 °C t = 0.54	4.7V	80:10:10 NMC111/Super C65/PVDF/$LiClO_4$ 1.5 mg cm^{-2}	25 °C, 0.3C, 3V–4.2V 1st discharge: 117.6 mAh g^{-1}. 200th discharge: 118.1 mAh g^{-1}. Coulombic efficiency close to 100%	[91]
PVDF-HFP -20% $Li_{6.4}Ga_{0.2}La_3Zr_2O$-TEP and FEC (7:3, v/v)-LiFSI	1.84×10^{-3} S cm^{-1} at 20 °C t = 0.563	4.75 V	80:5:10:5 NCM523/PVDF/Super-P 5 mg cm^{-2}	25 °C, 0.5C, 2.8–4.3 V 1st discharge: 96.3 mAh g^{-1}. 360th discharge: 90.522 mAh g^{-1}. Capacity retention: 94.08%. Coulombic efficiency~98%	[165]
PEO -12.5 vol% UiO-66-LiTFSI	3.1×10^{-5} S cm^{-1} at 25 °C 6.3×10^{-4} S cm^{-1} at 60 °C t = 0.72	4.97 V	50:30:10:10 LFM/LFP/LiTFSI/PEO/Super-P 2 mg cm^{-2}	LFP/Li: 60 °C, 1C, 2.8–3.8V 1st discharge: 106.3 mAh g^{-1}. 300th discharge: 90.78 mAh g^{-1}. Capacity retention: 85.4%. LFM/Li: 60 °C, 0.1C, 2.8–4.4V 100th discharge: 90.78 mAh g^{-1}. Capacity retention: 81.2%.	[103]
PVDF-HFP-12.5 wt% LLZTO-LiTFSI	8.80×10^{-5} S cm^{-1} at 25 °C t = 0.47	5V	80:10:10 LFP/PVDF-HFP/acetylene black 1.5 mg cm^{-2}	25 °C, 0.5C, 2.7–4.2 V 1st discharge: 101.4 mAh g^{-1}. 500th discharge: 110.9 mAh g^{-1}. Capacity retention: 99.5%. Coulombic efficiency~99.6%.	[97]
PEO -40% 3D Ga-LLZO-LiTFSI	1.2×10^{-4} S cm^{-1} at 30 °C t = 0.33	5.6V	75:10:10:5 LFP/PVDF/$LiClO_4$/carbon black	60 °C, 0.5C, 2.8–3.8 V 1st discharge: 138 mAh g^{-1}. 50th discharge: 128 mAh g^{-1}. Capacity retention: 92.1%. Coulombic efficiency: 99%.	[171]
PEO -1%$Li_{10}SnP_2S_{12}$-LiTFSI	1.69×10^{-4} S cm^{-1} at 50 °C	5.0V	40:15:45 S/LiTFSI/PEO/acetylene black 0.5 mg cm^{-2}	50 °C, 0.5C, 1.6V–2.8V 1st discharge: ~1016 mAh g^{-1}. 50th discharge: 1000 mAh g^{-1}. Capacity retention: 98.4%. Coulombic efficiency: ~100%.	[99]

(*continued on next page*)

Table 1 (*continued*)

Composite solid-state electrolyte	Ionic conductivity and Li^+ ion transference number	Electrochemical window	Cathode material and mass loading	Performance	Reference
PEO-20% P(SSPSILi-alt-MA)	3.08×10^{-4} S cm^{-1} at 25 °C t = 0.97 at 80 °C	5.0V	60:10:30 LFP/P(SSPSILi-alt-MA)/PEO/ carbon black	80 °C, 0.1C, 2.5–4V 1st discharge: 158.8 mAh g^{-1}. 100th discharge: 150.2 mAh g^{-1}. Capacity retention: 97.5%. Coulombic efficiency close to 100%	[84]
PEO -glass fiber-LiTFSI	1.9×10^{-4} S cm^{-1} at 60 °C	4.9V	80:10:10 vertically-aligned LFP/ PVDF-HFP/acetylene black 3 mg cm^{-2}	60 °C, 0.2C, 2.7 V–4.0 V 1st discharge: 145 mAh g^{-1}. 100th discharge: 155 mAh g^{-1}. Capacity retention: 100%. Coulombic efficiency: 100%	[172]
EGPEA -Nano fumed SiO_2-LiTFSI In situ polymerization	2.16×10^{-5} S cm^{-1} at 25 °C t = 0.63 at 55 °C	4.8V	80:10:10 LFP/PVDF/KB 2.5 mg cm^{-2}	55 °C, 0.1C, 2.5–4.0 V 1st discharge: 148 mAh g^{-1}, 95%. 100th discharge: 150.2 mAh g^{-1}. Capacity retention: 95%.	[100]
PEO-3.6 wt% 2D Ti_3C_2Tx-LiTFSI	2.2×10^{-5} S m^{-1} at 28 °C t = 0.18	4.7V	60 : 32: 8 LFP/CPOSS/carbon black 2.88 mg cm^{-2}	60 °C, 1/3C, 2.5V–4V 1st discharge: 140 mAh g^{-1}. Capacity retention 91.4%. Coulombic efficiency was >97%.	[98]
PEO-g-C_3N_4-LiTFSI	**1.7×10^{-5} S cm^{-1} at 30 °C t = 0.56**	**4.7V**	**80:10:10 LFP/PVDF/carbon black 1.2 mg cm^{-2}**	**60°C, 0.2 C, 2.8–4.0V 1st discharge: 161.1 mAh g^{-1}. 100th discharge: 155 mAh g^{-1}. Capacity retention: 96.2%. Coulombic efficiency: 99.5%**	[101]

which makes it difficult to conduct operando measurements in the liquid battery systems or even the solid-state polymer-based batteries. Therefore, the application of ND in solid-state batteries is still limited to ex situ test inorganic solid-state electrolytes.

In situ NDP is a typical technique to observe the spatial distribution and density of lithium during plating and stripping. Very recently, Wang et al. reported the formation mechanism of dendrites in LLZO and Li_3PS_4 by operando neutron depth profiling (NDP), which dynamically evaluated the distribution of Li^+ ion concentration in three common solid-state electrolytes of LiPON, LLZO and amorphous Li_3PS_4 during lithium deposition, and the growth mechanism of lithium dendrites was clearly explained [180]. Wagemaker et al. used operando NDP to monitor the lithium metal density and the evolution of inactive lithium in the solid electrolyte interphase layer during the electrochemical cycling of batteries, and successfully proved the importance of $LiNO_3$ as the additive of carbonate-based electrolytes for the stable operation of lithium metal [181]. In addition, the behavior of lithium metal deposition can also be observed by operando NDP. For instance, Li et al. employed operando NPD to quantitatively analyze the results of lithium metal deposition in three-dimensional structure electrode, in which the lithium metal deposition definitely relied on the deposition capacity [182]. In addition, operando NDP also can be used to monitor the degradation of batteries during charging and discharging [183].

3.6.2.2. Solid-state nuclear magnetic resonance (NMR). One of the most common applications of NMR in solid-state batteries is to study the lithium ion pathway by the observation of ^6Li and ^7Li [184]. Hu et al. has used NMR to deeply study the lithium ions pathway in the composite solid-state electrolyte of PEO/LLZO [42,45]. In addition, NMR can also be applied to explore Li^+ ion diffusion in inorganic solid-state electrolyte. Wilkening et al. recently used ^{31}P spin-lattice relaxation NMR to study the rotational jumps effect of PS_4^{3-} units on the fast Li^+ ion dynamics in Argyrodites Li_6PS_5X, which showed that the rotational dynamics of PS_4^{3-} with ordered anion sublattice in Li_6PS_5I is much faster than Li^+ ion self-diffusion [185]. For ex situ NMR, it is difficult to capture metastable structures and unstable products generated by LIBs electrode materials during electrochemical cycling. Therefore, it becomes particularly important to use in situ NMR technology, which can directly identify reaction types in real time during the charge/discharge process of solid-state batteries [186]. Nogami et al. used in situ ^{19}F NMR to reveal that the capacity attenuation in Li/PEO/$LiFePO_4$ solid-state batteries may be caused by local electrochemical polarization [187]. It should be noted that the presence of current and metals in the batteries make it difficult for the sample to rotate at a magic-angle under operando measurement, limiting the application of in situ NMR.

3.6.3. Characterization on electrodes/electrolyte interface

3.6.3.1. X-ray techniques. X-ray diffraction (XRD) is a common characterization method for structural characterization of solid-state materials. While the ex situ XRD is not applicable for some materials such as LiTFSI in solid-state electrolytes, whose state will change with the change of external conditions. In addition, it cannot monitor the structural changes of battery materials in the electrochemical process in real-time. Therefore, the in situ XRD technique has been developed to obtain the real-time information about electrochemical reactions in the batteries [188]. Koenig Jr et al. detected the formation of a stable ionic conductive interface layer between LAGP solid-state electrolyte and

high voltage active cathode material $LiMn_{1.5}Ni_{0.5}O_4$ (LMNO) by in situ XRD [189].

In solid-state LIBs, XPS has become another powerful technique for characterizing the interface information of solid-state electrolyte/lithium metal and solid-state electrolyte/cathode [190,191]. Compared with traditional XPS technique, using in situ XPS can dynamically study the chemical reaction at the interface and visually detect the reaction products in the electrochemical reaction. Teeter et al. revealed the instability between Li metal and Li_2S–P_2S_5 by using in situ XPS coupled with in situ Auger electron spectroscopy mapping [192]. As a technique to understand the failure mechanism of transient species and related electrodes at the dynamic molecular level, in situ XPS is crucial to accelerate the development of solid-state LIBs.

The time of flight-secondary ion mass spectrometer (TOF-SIMS) can characterize the information of element composition, molecular structure, molecular bond etc. on the surface of materials by measuring the flight time of secondary ions excited on the surface. Compared with other surface composition analysis techniques, the TOF-SIMS has the highest surface sensitivity, and can obtain the information of different molecules such as hexafluorophosphate (PF_6^-), lithium fluoride (LiF_2^-), $C_2H_3O_2^-$, etc. Moreover, high-resolution TOF-SIMS mapping can reveal the distribution of different components, which is an effective method to explore the composition of solid electrolyte interphase layer in batteries [193,194]. TOF-SIMS has been widely used in solid-state batteries as the most advanced tool for studying phase composition and microstructure [195]. More recently, Walther et al. characterized the interface of $LiNi_{0.6}Co_{0.2}Mn_{0.2}O_2$ and Li_6PS_5Cl by combining TOF-SIMS with X-ray photoelectron spectroscopy measurements, and revealed the local structure and morphology of solid electrolyte interphase layer for the first time [196]. This sophisticated technology provides valuable insights into the interphase composition and microstructure of solid-state batteries.

3.6.3.2. Image techniques. Specialized designed in situ SEM can be used to observe the morphology changes of electrodes/solid-state electrolytes. Li et al. observed the deposition behavior of lithium metal in solid-state batteries by in situ SEM and found that the morphology of lithium metal deposition was strong related to the capacity [182]. Zaghib et al. studied the capacity failure mechanism of Li–S solid-state battery during operation, and observed the dissolution of polysulfide to produce a catholyte through in situ SEM [197]. This non-destructive real-time observation technique is of great help to visually monitor battery failure.

In situ TEM can provide the real-time observation of the local changes of electrode materials at high spatial resolution. In addition to in situ TEM, spherical aberration corrected scanning transmission electron microscopy (STEM) combined with electron energy loss spectroscopy (EELS) has also made great progress in solid-state batteries recently, which can provide conclusive evidence of changes in electrode surface structure [198]. Chen et al. first applied a state-of-the-art chip-based in situ STEM holder to observe lithium plating/stripping behavior of solid-state $LiCoO_2$/LLZO/Li battery at the atomic scale, which accurately shows the single crystal $LiCoO_2$ tends to form polycrystalline phase at the nanoscale size during cycling [199]. Very recently, Nan et al. used STEM and observed that the lithium ion conductor LLTO and the Li-rich layered cathode tend to form an epitaxial interface, thus form a tight and sufficient solid-solid contact at the atomic scale. Through further in-depth analysis of the epitaxial interface, it was found that a mismatch dislocation would form at the interface at every 15 atomic planes, releasing the accumulated strain [154].

Cryo–electron microscopy (CE) is one kind of TEM that observe samples at low temperatures (up to −185 °C), which shows its advantages in the field of batteries. In 2017, Cui et al. first applied CE in LIBs and obtained atomic-level resolution images of lithium metal and solid electrolyte interphase layer, proving the possibility to conduct atomic resolution imaging of sensitive battery materials at low temperature [200]. In the process of using CE, the organic liquid electrolyte is rapidly frozen to vitrification, which is close to the nature of solid-state electrolytes [201,202]. Therefore, it is expect that CE is feasible for solid-state batteries for electrodes/electrolyte measure.

Operando X-ray tomography microscopy (XTM) is a 3D radiographic visualization technique, which can directly track the evolution of components and interface morphology. Operando XTM can dynamically monitor particle mechanical fracture and electrode fracture caused by volume expansion of solid electrodes active materials in solid-state lithium batteries during cycling without increasing external pressure. Manke et al. employed XTM to record the morphological and compositional evolution of In–Li-anode/sulfide solid-state electrolyte interface during battery cycling through operando XTM [203]. More recently, Villevieille et al. realized operando visualization of the electrochemical reaction gradient and morphological evolution in the interface composite layer in LTO/$75Li_2S$–$25P_2S_5$/Sn solid-state battery [204].

AFM (atomic force microscope) depends on the van der Waals force between the tip atoms and the sample surface atoms to feed back the sample surface morphology information. In solid-state batteries, AFM techniques display the unique advantages of flexible operation, facile sample preparation. AFM equipped with nanoprobe and STEM nanoprobe can be used to observe the mechanical properties and stress characteristics of solid-state electrolytes by combining with nanoindentation and TEM [179,205]. The AFM technique also shows unique advantages on the cathode/solid-state electrolyte interfacial potential measurements. Guo et al. studied the potential distribution from the NCM particles core to the inorganic lithium conductor LATP shell and poly (ether-acrylate) (ipn-PEA) electrolyte by AFM with peak force tapping mode to analyze the space charge layer [141]. In addition, in situ AFM techniques can also been employed to observe the transformation of cathode structure due to Li^+ ion intercalation [206,207]. Zhu et al. prepared TiO_2/LiPON/NCM solid-state batteries by magnetron sputtering, and obtained the high-resolution real-time space imaging on the NCM surface at different cycle stages by in situ AFM to reveal the correlation between ionic and electronic diffusion at the NCM cathode surface [206].

4. Conclusion and future perspectives

In summary, the solid-state lithium battery is promising to improve safety and achieve high energy density. Therefore, it has become an important direction of secondary lithium battery development. The key to solid-state batteries is to prepare solid-state electrolytes with wide electrochemical window, high room temperature ionic conductivity, high Li^+ ion transference number, low electrodes/electrolyte interface impedance. How to design composite solid-state electrolytes with homogeneous dual phase or multiphase components and stable interface, and guarantee the rapid transfer of Li^+ ion between different phases is a great challenge.

Although great efforts have been made to address the current issues of composite solid-state electrolytes, there is a long way to go before their practical application. Most solid-state batteries at the current development stage are still LFP-based and need to operate at high temperature. In addition, insufficient fundamental understanding of the ionic transport mechanism in dual phase or multiphase interface and interfacial process after charge/discharge hinders the development of solid-state electrolytes. Here, we provide some perspectives for the future development of composite solid-state electrolytes.

(1) Achieving high ionic conductivity and Li^+ ion transference number at room temperature is prerequisite for composite solid-state electrolytes. It is best to select components with both high intrinsic ionic conductivity and Li^+ ion transference number. Meanwhile, constructing fast Li^+ ion transport channels by the architecture design of solid-state electrolytes components is an

effective strategy for achieving excellent Li^+ ion transport properties. Therefore, developing new polymer matrix and inorganic components with excellent Li^+ ions transport ability, and exploring the best matching method between different components is quite significant. In addition, gaining in-depth understanding of Li^+ ion transport mechanisms can guide us to better design high-performance composite solid-state electrolytes. This is still a challenge, because the composite solid-state electrolytes is a dual phase or multiphase system and the interface transfer of Li^+ ion is more complex. In situ measurements, first-principles calculations, DFT and molecular dynamics, and finite element simulations will provide theoretical support for understanding the Li^+ ion transfer mechanism in composite solid-state electrolytes.

(2) Interfacial issues between composite solid-state electrolytes and electrodes are of great importance towards successful operation of solid-state lithium batteries. For cathode/electrolyte interface, with the continuous upgrade of cathode materials towards higher voltage, more attention should be paid to constructing voltage-resistance solid-state electrolytes or interfacial layers to better adapt to the high-voltage cathodes. For lithium anode/electrolyte interface, the major issue is the lithium dendrite growth/penetration through solid-state electrolytes. Constructing a lithium anode/electrolyte interface with high ionic conductivity, high Li^+ ion transference number and good viscoelasticity can effectively favor the uniform lithium deposition to restrain the lithium dendrite formation and growth. In addition, the contact loss at the interfaces caused by the volume change of electrodes is also a severe problem. Building a solid-state electrolytes framework to host electrodes and physically confine cathode and Li metal anode or constructing interfaces with good viscoelasticity are two effective methods for preventing or adapting the potential volume change of electrodes during charge-discharge process. Due to the difference between cathode/electrolyte and lithium anode/electrolyte interfaces, asymmetric or hierarchical structure may be a further trend of solid-state electrolytes.

(3) The characterization of solid-solid interface between two solid materials in working conditions is still a challenge. New battery configurations should be designed and advanced nondestructive characterization techniques should be developed to obtain real-time monitoring and analysis of interface composition and structure, as well as the Li^+ ion transfer mechanism at both solid-solid electrolyte components interface and electrodes/electrolyte interface in order to help us acquire a theoretical understanding of different solid-solid interfaces. Solid-state NMR and neutron technique are efficient methods to dynamically study the Li^+ ion transport and distribution in solid-state electrolytes in batteries. Operando X-ray techniques and visual image techniques provide a direct evidence to capture the reliable and accurate electrochemical reaction information at intervals of the batteries operation. The techniques used in liquid batteries, such as CE, AFM etc. are perspective to be developed in solid-state batteries [200].

(4) A single approach cannot resolve all issues of solid-state electrolytes and electrodes/electrolyte interfaces. The combination of comprehensive treatments, such as the surface and structure engineering of cathode and lithium metal anode, the architecture design of electrolytes, the electrodes/electrolyte interface engineering, should be considered. Although there have been numerous reports presenting the safety of solid-state batteries by cutting, puncturing and other damages, the comprehensive investigation on safety and failure mechanisms are still insufficient. The battery configuration should be adopted to achieve high-safety and high-performance of solid-state lithium metal batteries.

(5) The thickness of composite electrolytes in the existing literature is generally more than 100 μm, which is much thicker and heavier than liquid electrolyte/separator system. Therefore, solid-state electrolytes with thinner thickness, lower density, but excellent mechanical properties will be favorable for enhancing the energy density of batteries.

(6) As an ideal anode for rechargeable lithium batteries, lithium metal should maintain good stability after integrating with solid-state electrolytes. In practical battery operation, the interface between lithium metal anode and solid-state electrolytes is an important channel for Li + ion transport. The stability of lithium metal anode interface is expected to optimize the diffusion and distribution of Li^+ ion to achieve dendrite-free morphology and high utilization rate of lithium during cycling, which is of great significance to the long-term stability of solid-state LIBs. Therefore, effective lithium metal protection strategy is a good way to improve the performance of solid-state batteries and realize the transition from solid "point-point" contact to "face-face" contact. Some strategies such as adding Li-alloy interface layer, polymer flexible interface layer or artificial solid electrolyte interphase layer are feasible [208]. Recently, Archer et al. reported new solid-state electrolytes in situ generated on Li metal, which provides a new strategy for integrating solid-state electrolytes and lithium metal protection [209]. In addition, advanced manufacturing methods of solid-state electrolytes and solid-state batteries, such as 3D printing, electrostatic spinning etc. can be used to achieve specific structure and low bulk resistance of solid-state electrolytes membrane, so as to obtain the best electrolytes performance and solid-state batteries performance. In addition, miniaturization and integration of solid-state batteries will also be a tendency.

At present, the development of new energy storage devices and related materials is a booming field with both challenges and opportunities. The solid-state batteries are bound to be the main force in the next generation of energy storage devices. Composite solid-state electrolytes have great potential to be ultimate ideal electrolyte systems. We expect the rapid development of composite solid-state electrolytes can pave the way for practical applications of solid-state lithium batteries and facilitate the development of ionic conductive elements for other energy storage/conversion technologies.

Acknowledgment

The authors acknowledge the National Natural Science Foundation of China (21503131, 51711530162) and the Swedish Research Council.

Appendix A. Supplementary data

Supplementary data to this article can be found online at https://doi.org/10.1016/j.jpowsour.2019.227175.

References

[1] M. Armand, J.-M. Tarascon, Nature 451 (2008) 652–657.
[2] J.B. Goodenough, Energy Storage Materials 1 (2015) 158–161.
[3] X. Judez, G.G. Eshetu, C. Li, L.M. Rodriguez-Martinez, H. Zhang, M. Armand, Joule 2 (2018) 2208–2224.
[4] I. Thomas, F. Miller, Z.-G. Wang, G.W. Coates, N.P. Balsara, Acc. Chem. Res. 50 (2017) 590–593.
[5] S. Zhang, K. Ueno, K. Dokko, M. Watanabe, Adv. Energy Mater. 5 (2015) 1500117.
[6] J. Janek, W.G. Zeier, Nat. Energy. 1 (2016) 16141.
[7] D. Lei, K. Shi, H. Ye, Z. Wan, Y. Wang, L. Shen, B. Li, Q.-H. Yang, F. Kang, Y.-B. He, Adv. Funct. Mater. 28 (2018) 1707570.
[8] L. Fan, S. Wei, S. Li, Q. Li, Y. Lu, Adv. Energy Mater. 8 (2018) 1702657.
[9] R. Chen, W. Qu, X. Guo, L. Li, F. Wu, Mater. Horiz. 3 (2016) 487–516.
[10] P.G. Bruce, S.A. Freunberger, L.J. Hardwick, J.M. Tarascon, Nat. Mater. 11 (2011) 19–29.
[11] J. Yue, M. Yan, Y.-X. Yin, Y.-G. Guo, Adv. Funct. Mater. 28 (2018) 1707533.
[12] Y. Shen, Y. Zhang, S. Han, J. Wang, Z. Peng, L. Chen, Joule 2 (2018) 1674–1689.
[13] A. Manthiram, X. Yu, S. Wang, Nat. Rev. Mater. 2 (2017) 1–16.

[14] X.-B. Cheng, C.-Z. Zhao, Y.-X. Yao, H. Liu, Q. Zhang, Chem 5 (2019) 74–96.
[15] Q. Zhou, J. Zhang, G. Cui, Macromol. Mater. Eng. 303 (2018) 1800337.
[16] Q. Zhang, K. Liu, F. Ding, X. Liu, Nano Research 10 (2017) 4139–4174.
[17] H. Zhang, J. Zhang, J. Ma, G. Xu, T. Dong, G. Cui, Electrochem. Energy Rev. 2 (2019) 128–148.
[18] X. Ban, W. Zhang, N. Chen, C. Sun, J. Phys. Chem. C 122 (2018) 9852–9858.
[19] C. Wang, Y. Yang, X. Liu, H. Zhong, H. Xu, Z. Xu, H. Shao, F. Ding, ACS Appl. Mater. Interfaces 9 (2017) 13694–13702.
[20] Y.W. Chen-Yang, H.C. Chen, F.J. Lin, C.C. Chen, Solid State Ion. 150 (2002) 327–335.
[21] B.W. Zewde, L. Carbone, S. Greenbaum, J. Hassoun, Solid State Ion. 317 (2018) 97–102.
[22] L. Suo, O. Borodin, T. Gao, M. Olguin, J. Ho, X. Fan, C. Luo, C. Wang, K. Xu, Science 253 (2015) 938–943.
[23] Z. Zhang, Y. Shao, B. Lotsch, Y.-S. Hu, H. Li, J. Janek, L.F. Nazar, C.-W. Nan, J. Maier, M. Armand, L. Chen, Energy Environ. Sci. 11 (2018) 1945–1976.
[24] N. Kamaya, K. Homma, Y. Yamakawa, M. Hirayama, R. Kanno, M. Yonemura, T. Kamiyama, Y. Kato, S. Hama, K. Kawamoto, A. Mitsui, Nat. Mater. 10 (2011) 682–686.
[25] P. Bron, S. Johansson, K. Zick, J. Schmedt auf der Gunne, S. Dehnen, B. Roling, J. Am. Chem. Soc. 135 (2013) 15694–15697.
[26] X. Xu, Z. Wen, X. Yang, J. Zhang, Z. Gu, Solid State Ion. 177 (2006) 2611–2615.
[27] M. Yashima, M. Itoh, Y. Inaguma, Y. Morii, J. Am. Chem. Soc. 127 (2005) 3491–3495.
[28] V. Thangadurai, S. Narayanan, D. Pinzaru, Chem. Soc. Rev. 43 (2014) 4714–4727.
[29] Y. Meesala, A. Jena, H. Chang, R.-S. Liu, ACS Energy Lett 2 (2017) 2734–2751.
[30] J. Yu, Y.-Q. Lyu, J. Liu, M.B. Effat, S.C.T. Kwok, J. Wu, F. Ciucci, J. Mater. Chem. A. 7 (2019) 17995–18002.
[31] J. Wan, J. Xie, X. Kong, Z. Liu, K. Liu, F. Shi, A. Pei, H. Chen, W. Chen, J. Chen, X. Zhang, Linqi Zong, J. Wang, L.-Q. Chen, J. Qin, Y. Cui, Nat. Nanotechnol. 14 (2019) 705–711.
[32] W. Zhou, H. Gao, J.B. Goodenough, Adv. Energy Mater. 6 (2016) 1501802.
[33] J. Wan, J. Xie, D.G. Mackanic, W. Burke, Z. Bao, Y. Cui, Materials Today Nano 4 (2018) 1–16.
[34] J. Lopez, D.G. Mackanic, Y. Cui, Z. Bao, Nat. Rev. Mater. 4 (2019) 312–330.
[35] M.F. Lagadec, R. Zahn, V. Wood, Nat. Energy. 4 (2018) 16–25.
[36] B. Commarieu, A. Paolella, J.-C. Daigle, K. Zaghib, Current Opinion in Electrochem 9 (2018) 56–63.
[37] H. Zhang, C. Li, M. Piszcz, E. Coya, T. Rojo, L.M. Rodriguez-Martinez, M. Armand, Z. Zhou, Chem. Soc. Rev. 46 (2017) 797–815.
[38] R. Bouchet1, S. Maria, R. Meziane, A. Aboulaich, L. Lienafa, J.-P. Bonnet, T.N. T. Phan, D. Bertin, D. Gigmes, D. Devaux, R. Denoyel, M. Armand, Nat. Mater. 12 (2013) 452–457.
[39] S. Li, A.I. Mohamed, V. Pande, H. Wang, J. Cuthbert, X. Pan, H. He, Z. Wang, V. Viswanathan, J.F. Whitacre, K. Matyjaszewski, ACS Energy Lett 3 (2017) 20–27.
[40] J. Mindemark, M.J. Lacey, T. Bowden, D. Brandell, Prog. Polym. Sci. 81 (2018) 114–143.
[41] M. Keller, A. Varzi, S. Passerini, J. Power Sources 392 (2018) 206–225.
[42] J. Zheng, M. Tang, Y.Y. Hu, Angew. Chem. Int. Ed. 55 (2016) 12538–12542.
[43] T. Yang, J. Zheng, Q. Cheng, Y.Y. Hu, C.K. Chan, ACS Appl. Mater. Interfaces 9 (2017) 21773–21780.
[44] L. Chen, Y. Li, S.-P. Li, L.-Z. Fan, C.-W. Nan, J.B. Goodenough, Nano Energy 46 (2018) 176–184.
[45] J. Zheng, Y.Y. Hu, ACS Appl. Mater. Interfaces 10 (2018) 4113–4120.
[46] S. Xin, Y. You, S. Wang, H.-C. Gao, Y.-X. Yin, Y.-G. Guo, ACS Energy Lett 2 (2017) 1385–1394.
[47] S.S. Zhang, ACS Appl. Energy Mater. 1 (2018) 910–920.
[48] M. Armand, Solid State Ion. 9–10 (1983) 745–754.
[49] J.M. Parker, P.V. Wright, Polymer 14 (1973) 589.
[50] E.M. Masoud, A.A. El-Bellihi, W.A. Bayoumy, M.A. Mousa, J. Alloy. Comp. 575 (2013) 223–228.
[51] X. Wang, Y. Zhang, X. Zhang, T. Liu, Y.H. Lin, L. Li, Y. Shen, C.W. Nan, ACS Appl. Mater. Interfaces 10 (2018) 24791–24798.
[52] T. Zhang, N. Imanishi, S. Hasegawa, A. Hirano, J. Xie, Y. Takeda, O. Yamamoto, N. Sammes, Electrochem. Solid State Lett. 12 (2009) A132.
[53] J.L. Nugent, S.S. Moganty, L.A. Archer, Adv. Mater. 22 (2010) 3677–3680.
[54] F. Croce, G.B. Appetecchi, L. Persi, B. Scrosati, Nature 394 (1998) 456–458.
[55] P. Pal, A. Ghosh, Electrochim. Acta 260 (2018) 157–167.
[56] J.L. Lutkenhaus, E.A. Olivetti, E.A. Verploegen, B.M. Cord, D.R. Sadoway, P. T. Hammond, Langmuir 23 (2007) 8515–8521.
[57] Y. Tominaga, K. Yamazaki, Chem. Commun. 50 (2014) 4448–4450.
[58] E. Masdupuy, Ann. Chim. 13 (1957) 527–586.
[59] W. Liu, N. Liu, J. Sun, P.C. Hsu, Y. Li, H.W. Lee, Y. Cui, Nano Lett. 15 (2015) 2740–2745.
[60] Y. Li, W. Zhang, Q. Dou, K.W. Wong, K.M. Ng, J. Mater. Chem. 7 (2019) 3391–3398.
[61] Q. Guo, Y. Han, H. Wang, S. Xiong, Y. Li, S. Liu, K. Xie, ACS Appl. Mater. Interfaces 9 (2017) 41837–41844.
[62] G. Hou, X. Ma, Q. Sun, Q. Ai, X. Xu, L. Chen, D. Li, J. Chen, H. Zhong, Y. Li, Z. Xu, P. Si, J. Feng, L. Zhang, F. Ding, L. Ci, ACS Appl. Mater. Interfaces 10 (2018) 18610–18618.
[63] J. Zhang, N. Zhao, M. Zhang, Y. Li, P.K. Chu, X. Guo, Z. Di, X. Wang, H. Li, Nano Energy 28 (2016) 447–454.
[64] R.C. Agrawal, R.K. Gupta, J. Mater. Sci. 34 (1999) 1131–1162.
[65] C.C. Liang, J. Electrochem. Soc. 120 (1973) 1289.
[66] W. Liu, S.W. Lee, D. Lin, F. Shi, S. Wang, A.D. Sendek, Y. Cui, Nat. Energy. 2 (2017) 1–7.
[67] H. Zhai, P. Xu, M. Ning, Q. Cheng, J. Mandal, Y. Yang, Nano Lett. 17 (2017) 3182–3187.
[68] X. Liu, S. Peng, S. Gao, Y. Cao, Q. You, L. Zhou, Y. Jin, Z. Liu, J. Liu, ACS Appl. Mater. Interfaces 10 (2018) 15691–15696.
[69] X. Wang, H. Zhai, B. Qie, Q. Cheng, A. Li, J. Borovilas, B. Xu, C. Shi, T. Jin, X. Liao, Y. Li, X. He, S. Du, Y. Fu, M. Dontigny, K. Zaghib, Y. Yang, Nano Energy 60 (2019) 205–212.
[70] J. Bae, Y. Li, J. Zhang, X. Zhou, F. Zhao, Y. Shi, J.B. Goodenough, G. Yu, Angew. Chem. Int. Ed. 57 (2018) 2096–2100.
[71] J. Bae, Y. Li, F. Zhao, X. Zhou, Y. Ding, G. Yu, Energy Storage Materials 15 (2018) 46–52.
[72] C. Yang, L. Zhang, B. Liu, S. Xu, T. Hamann, D. McOwen, J. Dai, W. Luo, Y. Gong, E.D. Wachsman, L. Hu, Proc. Natl. Acad. Sci. Unit. States Am. 115 (2018) 3770–3775.
[73] Z. Huang, W. Pang, P. Liang, Z. Jin, N.S. Grundish, Y. Li, C. Wang, J. Mater. Chem. 7 (2019) 16425–16436.
[74] X. Zhang, T. Liu, S. Zhang, X. Huang, B. Xu, Y. Lin, B. Xu, L. Li, C.W. Nan, Y. Shen, J. Am. Chem. Soc. 139 (2017) 13779–13785.
[75] X. Zhang, J. Xie, F. Shi, D. Lin, Y. Liu, W. Liu, A. Pei, Y. Gong, H. Wang, K. Liu, Y. Xiang, Y. Cui, Nano Lett. 18 (2018) 3829–3838.
[76] L. Chen, W. Li, L.Z. Fan, C.W. Nan, Q. Zhang, Adv. Funct. Mater. (2019) 1901047.
[77] Y. Du, H. Yang, J.M. Whiteley, S. Wan, Y. Jin, S.H. Lee, W. Zhang, Angew. Chem. Int. Ed. 55 (2016) 1737–1741.
[78] H. Chen, H. Tu, C. Hu, Y. Liu, D. Dong, Y. Sun, Y. Dai, S. Wang, H. Qian, Z. Lin, L. Chen, J. Am. Chem. Soc. 140 (2018) 896–899.
[79] Y. Hu, N. Dunlap, S. Wan, S. Lu, S. Huang, I. Sellinger, M. Ortiz, Y. Jin, S.H. Lee, W. Zhang, J. Am. Chem. Soc. 141 (2019) 7518−−7525.
[80] Q. Xu, S. Tao, Q. Jiang, D. Jiang, J. Am. Chem. Soc. 140 (2018) 7429–7432.
[81] W. Zhou, S. Wang, Y. Li, S. Xin, A. Manthiram, J.B. Goodenough, J. Am. Chem. Soc. 138 (2016) 9385–9388.
[82] Y. Li, B. Xu, H. Xu, H. Duan, X. Lu, S. Xin, W. Zhou, L. Xue, G. Fu, A. Manthiram, J.B. Goodenough, Angew. Chem. Int. Ed. 56 (2017) 753–756.
[83] Z. Zhang, Y. Zhao, S. Chen, D. Xie, X. Yao, P. Cui, X. Xu, J. Mater. Chem. 5 (2017) 16984–16993.
[84] C. Cao, Y. Li, Y. Feng, C. Peng, Z. Li, W. Feng, Energy Storage Materials 19 (2019) 401–407.
[85] C. Cao, Y. Li, Y. Feng, P. Long, H. An, C. Qin, J. Han, S. Li, W. Feng, J. Mater. Chem. 5 (2017) 22519–22526.
[86] S.S. Park, Y. Tulchinsky, M. Dinca, J. Am. Chem. Soc. 139 (2017) 13260–13263.
[87] G. Luo, B. Yuan, T. Guan, F. Cheng, W. Zhang, J. Chen, ACS Appl. Energy Mater. 2 (2019) 3028–3034.
[88] D. Xu, J. Su, J. Jin, C. Sun, Y. Ruan, C. Chen, Z. Wen, Adv. Energy Mater. (2019) 1900611.
[89] J. Zhang, X. Zang, H. Wen, T. Dong, J. Chai, Y. Li, B. Chen, J. Zhao, S. Dong, J. Ma, L. Yue, Z. Liu, X. Guo, G. Cui, L. Chen, J. Mater. Chem. 5 (2017) 4940–4948.
[90] Y. Zhang, W. Lu, L. Cong, J. Liu, L. Sun, A. Mauger, C.M. Julien, H. Xie, J. Liu, J. Power Sources 420 (2019) 63–72.
[91] P. Yao, B. Zhu, H. Zhai, X. Liao, Y. Zhu, W. Xu, Q. Cheng, C. Jayyosi, Z. Li, J. Zhu, K.M. Myers, X. Chen, Y. Yang, Nano Lett. 18 (2018) 6113–6120.
[92] D. Lin, P.Y. Yuen, Y. Liu, W. Liu, N. Liu, R.H. Dauskardt, Y. Cui, Adv. Mater. 30 (2018), e1802661.
[93] D. Zhang, L. Zhang, K. Yang, H. Wang, C. Yu, D. Xu, B. Xu, L.M. Wang, ACS Appl. Mater. Interfaces 9 (2017) 36886–36896.
[94] W. Tang, S. Tang, X. Guan, X. Zhang, Q. Xiang, J. Luo, Adv. Funct. Mater. 29 (2019) 1900648.
[95] Z. Li, W.X. Sha, X. Guo, ACS Appl. Mater. Interfaces 11 (2019) 26920–26927.
[96] Z. Wang, Z. Wang, L. Yang, H. Wang, Y. Song, L. Han, K. Yang, J. Hu, H. Chen, F. Pan, Nano Energy 49 (2018) 580–587.
[97] J. Lu, Y. Liu, P. Yao, Z. Ding, Q. Tang, J. Wu, Z. Ye, K. Huang, X. Liu, Chem. Eng. J. 367 (2019) 230–238.
[98] Q. Pan, Y. Zheng, S. Kota, W. Huang, S. Wang, H. Qi, S. Kim, Y. Tu, M. W. Barsoum, C.Y. Li, Nanoscale Adv 1 (2019) 395–402.
[99] X. Li, D. Wang, H. Wang, H. Yan, Z. Gong, Y. Yang, ACS Appl. Mater. Interfaces 11 (2019) 22745–22753.
[100] C. Niu, J. Liu, G. Chen, C. Liu, T. Qian, J. Zhang, B. Cao, W. Shang, Y. Chen, J. Han, J. Du, Y. Chen, J. Power Sources 417 (2019) 70–75.
[101] Z. Sun, Y. Li, S. Zhang, L. Shi, H. Wu, H. Bu, S. Ding, J. Mater. Chem. 7 (2019) 11069–11076.
[102] C.Z. Zhao, X.Q. Zhang, X.B. Cheng, R. Zhang, R. Xu, P.Y. Chen, H.J. Peng, J. Q. Huang, Q. Zhang, Proc. Natl. Acad. Sci. Unit. States Am. 114 (2017) 11069–11074.
[103] H. Huo, B. Wu, T. Zhang, X. Zheng, L. Ge, T. Xu, X. Guo, X. Sun, Energy Storage Materials 18 (2019) 59–67.
[104] S. Xia, X. Wu, Z. Zhang, Y. Cui, W. Liu, Chem 5 (2019) 753–785.
[105] S.-S. Chi, Y. Liu, N. Zhao, X. Guo, C.-W. Nan, L.-Z. Fan, Energy Storage Materials 17 (2019) 309–316.
[106] W. Zhou, Y. Zhu, N. Grundish, X. Sen, S. Wang, Y. You, N. Wu, J. Gao, Z. Cui, Y. Li, J.B. Goodenough, Nano Energy 53 (2018) 926–931.
[107] D. Dong, B. Zhou, Y. Sun, H. Zhang, G. Zhong, Q. Dong, F. Fu, H. Qian, Z. Lin, D. Lu, Y. Shen, J. Wu, L. Chen, H. Chen, Nano Lett. 19 (2019) 2343–2349.
[108] B. Liu, Y. Gong, K. Fu, X. Han, Y. Yao, G. Pastel, C. Yang, H. Xie, E.D. Wachsman, L. Hu, ACS Appl. Mater. Interfaces 9 (2017) 18809–18815.

[109] Q. Yu, D. Han, Q. Lu, Y.B. He, S. Li, Q. Liu, C. Han, F. Kang, B. Li, ACS Appl. Mater. Interfaces 11 (2019) 9911–9918.
[110] H. Huo, N. Zhao, J. Sun, F. Du, Y. Li, X. Guo, J. Power Sources 372 (2017) 1–7.
[111] Q. Ma, X.X. Zeng, J. Yue, Y.X. Yin, T.T. Zuo, J.Y. Liang, Q. Deng, X.W. Wu, Y. G. Guo, Adv. Energy Mater. 9 (2019) 1803854.
[112] M. Rosso, T. Gobron, C. Brissot, J.-N. Chazalviel, S. Lascaud, J. Power Sources 97–98 (2001) 804–806.
[113] C. Brissot, M. Rosso, J.-N.C.S. Lascaud, J. Power Sources 81–82 (1999) 925–929.
[114] D. Gunceler, K. Letchworth-Weaver, R. Sundararaman, K.A. Schwarz, T.A. Arias, Model. Simul. Mater. Sci. Eng. 21 (2013), 074005.
[115] P. Bai, J. Li, F.R. Brushett, M.Z. Bazant, Energy Environ. Sci. 9 (2016) 3221–3229.
[116] R. Jin, L. Fu, H. Zhou, Z. Wang, Z. Qiu, L. Shi, J. Zhu, S. Yuan, ACS Sustain. Chem. Eng. 6 (2018) 2961–2968.
[117] J. Chai, B. Chen, F. Xian, P. Wang, H. Du, J. Zhang, Z. Liu, H. Zhang, S. Dong, X. Zhou, G. Cui, Small 14 (2018), e1802244.
[118] J. Ju, Y. Wang, B. Chen, J. Ma, S. Dong, J. Chai, H. Qu, L. Cui, X. Wu, G. Cui, ACS Appl. Mater. Interfaces 10 (2018) 13588–13597.
[119] J. Chai, Z. Liu, J. Ma, J. Wang, X. Liu, H. Liu, J. Zhang, G. Cui, L. Chen, Adv. Sci. 4 (2017) 1600377.
[120] D. Zhou, Y.-B. He, Q. Cai, X. Qin, B. Li, H. Du, Q.-H. Yang, F. Kang, J. Mater. Chem. 2 (2014) 20059–20066.
[121] D. Zhou, Y.-B. He, R. Liu, M. Liu, H. Du, B. Li, Q. Cai, Q.-H. Yang, F. Kang, Adv. Energy Mater. 5 (2015) 1500353.
[122] L. Liu, L. Chu, B. Jiang, M. Li, Solid State Ion. 331 (2019) 89–95.
[123] Z. He, L. Chen, B. Zhang, Y. Liu, L.-Z. Fan, J. Power Sources 392 (2018) 232–238.
[124] X.X. Zeng, Y.X. Yin, N.W. Li, W.C. Du, Y.G. Guo, L.J. Wan, J. Am. Chem. Soc. 138 (2016) 15825–15828.
[125] F. Boujioui, F. Zhuge, H. Damerow, M. Wehbi, B. Améduri, J.-F. Gohy, J. Mater. Chem. 6 (2018) 8514–8522.
[126] D. Li, L. Chen, T. Wang, L.Z. Fan, ACS Appl. Mater. Interfaces 10 (2018) 7069–7078.
[127] X. Han, Y. Gong, K.K. Fu, X. He, G.T. Hitz, J. Dai, A. Pearse, B. Liu, H. Wang, G. Rubloff, Y. Mo, V. Thangadurai, E.D. Wachsman, L. Hu, Nat. Mater. 16 (2017) 572–579.
[128] S. Xu, D.W. McOwen, C. Wang, L. Zhang, W. Luo, C. Chen, Y. Li, Y. Gong, J. Dai, Y. Kuang, C. Yang, T.R. Hamann, E.D. Wachsman, L. Hu, Nano Lett. 18 (2018) 3926–3933.
[129] J. Liang, Q. Sun, Y. Zhao, Y. Sun, C. Wang, W. Li, M. Li, D. Wang, X. Li, Y. Liu, K. Adair, R. Li, L. Zhang, R. Yang, S. Lu, H. Huang, X. Sun, J. Mater. Chem. 6 (2018) 23712–23719.
[130] Y. Gong, K. Fu, S. Xu, J. Dai, T.R. Hamann, L. Zhang, G.T. Hitz, Z. Fu, Z. Ma, D. W. McOwen, X. Han, L. Hu, E.D. Wachsman, Mater. Today 21 (2018) 594–601.
[131] H. Huo, Y. Chen, J. Luo, X. Yang, X. Guo, X. Sun, Adv. Energy Mater. 9 (2019) 1804004.
[132] J.M. Whiteley, P. Taynton, W. Zhang, S.-H. Lee, Adv. Mater. 27 (2015) 6922–6927.
[133] B. Zhou, C. Zuo, Z. Xiao, X. Zhou, D. He, X. Xie, Z. Xue, Chem 24 (2018) 19200–19207.
[134] S. Xia, J. Lopez, C. Liang, Z. Zhang, Z. Bao, Y. Cui, W. Liu, Adv. Sci. 6 (2019) 1802353.
[135] J. Lopez, Y. Sun, D.G. Mackanic, M. Lee, A.M. Foudeh, M.S. Song, Y. Cui, Z. Bao, Adv. Mater. 30 (2018), e1804142.
[136] W. Wei, Z. Xu, L. Xu, X. Zhang, H. Xiong, J. Yang, ACS Appl. Energy Mater. 1 (2018) 6769–6773.
[137] W. Liu, J. Chen, Z. Chen, K. Liu, G. Zhou, Y. Sun, M.-S. Song, Z. Bao, Y. Cui, Adv. Energy Mater. 7 (2017) 1701076.
[138] B. Zhang, P. Zhang, H. Zhang, C. Yan, Z. Zheng, B. Wu, Y. Yu, Macromol. Rapid Commun. 38 (2017) 1700110.
[139] W. Chen, T. Lei, C. Wu, M. Deng, C. Gong, K. Hu, Y. Ma, L. Dai, W. Lv, W. He, X. Liu, J. Xiong, C. Yan, Adv. Energy Mater. 8 (2018) 1702348.
[140] X. Chen, P.M. Vereecken, Adv. Mater. Interfaces. 6 (2018) 1800899.
[141] J.Y. Liang, X.X. Zeng, X.D. Zhang, P.F. Wang, J.Y. Ma, Y.X. Yin, X.W. Wu, Y. G. Guo, L.J. Wan, J. Am. Chem. Soc. 140 (2018) 6767–6770.
[142] L.-P. Wang, X.-D. Zhang, T.-S. Wang, Y.-X. Yin, J.-L. Shi, C.-R. Wang, Y.-G. Guo, Adv. Energy Mater. 8 (2018) 1801528.
[143] Jun Ma, Z. Liu, B. Chen, Longlong Wang, L. Yue, H. Liu, J. Zhang, Z. Liu, G. Cu, J. Electrochem. Soc. 164 (14) (2017) A3454–A3461.
[144] R. Tan, J. Yang, J. Zheng, K. Wang, L. Lin, S. Ji, J. Liu, F. Pan, Nano Energy 16 (2015) 112–121.
[145] S. Chen, K. Wen, J. Fan, Y. Bando, D. Golberg, J. Mater. Chem. 6 (2018) 11631–11663.
[146] W. Dong, X.X. Zeng, X.D. Zhang, J.Y. Li, J.L. Shi, Y. Xiao, Y. Shi, R. Wen, Y.X. Yin, T.S. Wang, C.R. Wang, Y.G. Guo, ACS Appl. Mater. Interfaces 10 (2018) 18005–18011.
[147] C. Wang, G. Bai, Y. Yang, X. Liu, H. Shao, Nano Research 12 (2018) 217–223.
[148] Y. Li, F. Ding, Z. Xu, L. Sang, L. Ren, W. Ni, X. Liu, J. Power Sources 397 (2018) 95–101.
[149] H. Duan, Y.-X. Yin, X.-X. Zeng, J.-Y. Li, J.-L. Shi, Y. Shi, R. Wen, Y.-G. Guo, L.-J. Wan, Energy Storage Materials 10 (2018) 85–91.
[150] Z. Wan, D. Lei, W. Yang, C. Liu, K. Shi, X. Hao, L. Shen, W. Lv, B. Li, Q.-H. Yang, F. Kang, Y.-B. He, Adv. Funct. Mater. 29 (2019) 1805301.
[151] X. Chen, W. He, L.-X. Ding, S. Wang, H. Wang, Energy Environ. Sci. 12 (2019) 938–944.
[152] K. Fu, Y. Gong, G.T. Hitz, D.W. McOwen, Y. Li, S. Xu, Y. Wen, L. Zhang, C. Wang, G. Pastel, J. Dai, B. Liu, H. Xie, Y. Yao, E.D. Wachsman, L. Hu, Energy Environ. Sci. 10 (2017) 1568–1575.
[153] X. Tao, Y. Liu, W. Liu, G. Zhou, J. Zhao, D. Lin, C. Zu, O. Sheng, W. Zhang, H. W. Lee, Y. Cui, Nano Lett. 17 (2017) 2967–2972.
[154] F. Li, J. Li, F. Zhu, T. Liu, B. Xu, T.-H. Kim, M.J. Kramer, C. Ma, L. Zhou, C.-W. Nan, Matter 1 (2019) 1–16.
[155] Y. Zhu, J. Cao, H. Chen, Q. Yu, B. Li, J. Mater. Chem. 7 (2019) 6832–6839.
[156] L. Yang, Z. Wang, Y. Feng, R. Tan, Y. Zuo, R. Gao, Y. Zhao, L. Han, Z. Wang, F. Pan, Adv. Energy Mater. 7 (2017) 1701437.
[157] D. Lin, W. Liu, Y. Liu, H.R. Lee, P.C. Hsu, K. Liu, Y. Cui, Nano Lett. 16 (2016) 459–465.
[158] L. Porcarelli, C. Gerbaldi, F. Bella, J.R. Nair, Sci. Rep. 6 (2016) 19892.
[159] J. Hu, W. Wang, H. Peng, M. Guo, Y. Feng, Z. Xue, Y. Ye, X. Xie, Macromolecules 50 (2017) 1970–1980.
[160] M. Falco, L. Castro, J.R. Nair, F. Bella, F. Bardé, G. Meligrana, C. Gerbaldi, ACS Appl. Energy Mater. 2 (2019) 1600–1607.
[161] LipingWang BoWu, Z. Li, M. Zhao, K. Chen, S. Liu, Y. Pu, J. Li, J. Electrochem. Soc. 163 (10) (2016) A2248–A2252.
[162] S. Patel, R. Kumar Nidhi, J. Alloy. Comp. 789 (2019) 6–14.
[163] Y. Saito, H. Kataoka, E. Quartarone, P. Mustarelli, J. Phys. Chem. B 106 (2002) 7200–7204.
[164] W. Zhang, J. Nie, F. Li, Z.L. Wang, C. Sun, Nano Energy 45 (2018) 413–419.
[165] D. Xu, J. Su, J. Jin, C. Sun, Y. Ruan, C. Chen, Z. Wen, Adv. Energy Mater. (2019) 1900611.
[166] K. Nie, Y. Hong, J. Qiu, Q. Li, X. Yu, H. Li, L. Chen, Front Chem 6 (2018) 616.
[167] H. Duan, Y.X. Yin, Y. Shi, P.F. Wang, X.D. Zhang, C.P. Yang, J.L. Shi, R. Wen, Y. G. Guo, L.J. Wan, J. Am. Chem. Soc. 140 (2018) 82–85.
[168] W. Zhou, Z. Wang, Y. Pu, Y. Li, S. Xin, X. Li, J. Chen, J.B. Goodenough, Adv. Mater. 31 (2019), e1805574.
[169] H. Duan, M. Fan, W.P. Chen, J.Y. Li, P.F. Wang, W.P. Wang, J.L. Shi, Y.X. Yin, L. J. Wan, Y.G. Guo, Adv. Mater. 31 (2019), e1807789.
[170] J.Y. Liang, X.X. Zeng, X.D. Zhang, T.T. Zuo, M. Yan, Y.X. Yin, J.L. Shi, X.W. Wu, Y. G. Guo, L.J. Wan, J. Am. Chem. Soc. 141 (2019) 9165–9169.
[171] Z. Li, W.X. Sha, X. Guo, ACS Appl. Mater. Interfaces 11 (2019) 26920–26927.
[172] X. Yang, Q. Sun, C. Zhao, X. Gao, K.R. Adair, Y. Liu, J. Luo, X. Lin, J. Liang, H. Huang, L. Zhang, R. Yang, S. Lu, R. Li, X. Sun, Nano Energy 61 (2019) 567–575.
[173] A.M. Nolan, Y. Zhu, X. He, Q. Bai, Y. Mo, Joule 2 (2018) 2016–2046.
[174] Q. Bai, L. Yang, H. Chen, Y. Mo, Adv. Energy Mater. 8 (2018) 1702998.
[175] J. Yang, J.S. Tse, Comput. Mater. Sci. 107 (2015) 134–138.
[176] S. Sicolo, C. Kalcher, S.J. Sedlmaier, J. Janek, K. Albe, Solid State Ion. 319 (2018) 83–91.
[177] Z. Deng, B. Radhakrishnan, S.P. Ong, Chem. Mater. 27 (2015) 3749–3755.
[178] L.E. Camacho-Forero, P.B. Balbuena, J. Power Sources 396 (2018) 782–790.
[179] D. Liu, Z. Shadike, R. Lin, K. Qian, H. Li, K. Li, S. Wang, Q. Yu, M. Liu, S. Ganapathy, X. Qin, Q.H. Yang, M. Wagemaker, F. Kang, X.Q. Yang, B. Li, Adv. Mater. 31 (2019), e1806620.
[180] F. Han, A.S. Westover, J. Yue, X. Fan, F. Wang, M. Chi, D.N. Leonard, N. J. Dudney, H. Wang, C. Wang, Nat. Energy. 4 (2019) 187–196.
[181] M. Liu, Z. Cheng, K. Qian, T. Verhallen, C. Wang, M. Wagemaker, Chem. Mater. 31 (2019) 4564–4574.
[182] Q. Li, T. Yi, X. Wang, H. Pan, B. Quan, T. Liang, X. Guo, X. Yu, H. Wang, X. Huang, L. Chen, H. Li, Nano Energy 63 (2019) 103895.
[183] C. Chen, J.F.M. Oudenhoven, D.L. Danilov, E. Vezhlev, L. Gao, N. Li, F.M. Mulder, R.-A. Eichel, P.H.L. Notten, Adv. Energy Mater. 8 (2018) 1801430.
[184] E. Zhao, K. Nie, X. Yu, Y.-S. Hu, F. Wang, J. Xiao, H. Li, X. Huang, Adv. Funct. Mater. 28 (2018) 1707543.
[185] I. Hanghofer, B. Gadermaier, H.M.R. Wilkening, Chem. Mater. 31 (2019) 4591–4597.
[186] G.-L. Xu, H. Sun, C. Luo, L. Estevez, M. Zhuang, H. Gao, R. Amine, H. Wang, X. Zhang, C.-J. Sun, Y. Liu, Y. Ren, S.M. Heald, C. Wang, Z. Chen, K. Amine, Adv. Energy Mater. 9 (2019) 1802235.
[187] M. Nakayama, S. Wada, S. Kuroki, M. Nogami, Energy Environ. Sci. 3 (2010) 1995–2002.
[188] E. Hirose, K. Niwa, K. Kataoka, J. Akimoto, M. Hasegawa, Mater. Res. Bull. 107 (2018) 361–365.
[189] J.P. Robinson, P.D. Kichambare, J.L. Deiner, R. Miller, M.A. Rottmayer, G. M. Koenig, J. Am. Ceram. Soc. 101 (2018) 1087–1094.
[190] L. Sang, K.L. Bassett, F.C. Castro, M.J. Young, L. Chen, R.T. Haasch, J.W. Elam, V. P. Dravid, R.G. Nuzzo, A.A. Gewirth, Chem. Mater. 30 (2018) 8747–8756.
[191] M. Fingerle, R. Buchheit, S. Sicolo, K. Albe, R. Hausbrand, Chem. Mater. 29 (2017) 7675–7685.
[192] K.N. Wood, K.X. Steirer, S.E. Hafner, C. Ban, S. Santhanagopalan, S.H. Lee, G. Teeter, Nat. Commun. 9 (2018) 2490.
[193] E.Y. Jung, C.-S. Park, J.C. Lee, E. Pazhetnov, K.J. Suh, S. Heo, T.E. Hong, D.H. Lee, S.-I. Chien, H.-S. Tae, Mol. Cryst. Liq. Cryst. 663 (2018) 158–167.
[194] C. Fiedler, B. Luerssen, M. Rohnke, J. Sann, J. Janek, J. Electrochem. Soc. 164 (14) (2017) A3742–A3749.
[195] Y. Li, X. Chen, A. Dolocan, Z. Cui, S. Xin, L. Xue, H. Xu, K. Park, J.B. Goodenough, J. Am. Chem. Soc. 140 (2018) 6448–6455.
[196] F. Walther, R. Koerver, T. Fuchs, S. Ohno, J. Sann, M. Rohnke, W.G. Zeier, J. Janek, Chem. Mater. 31 (2019) 3745–3755.
[197] H. Marceau, C.-S. Kim, A. Paolella, S. Ladouceur, M. Lagacé, M. Chaker, A. Vijh, A. Guerfi, C.M. Julien, A. Mauger, M. Armand, P. Hovington, K. Zaghib, J. Power Sources 319 (2016) 247–254.
[198] X. Liu, L. Gu, Small Methods 2 (2018) 1800006.
[199] Y. Gong, J. Zhang, L. Jiang, J.A. Shi, Q. Zhang, Z. Yang, D. Zou, J. Wang, X. Yu, R. Xiao, Y.S. Hu, L. Gu, H. Li, L. Chen, J. Am. Chem. Soc. 139 (2017) 4274–4277.

[200] Y. Li, Y. Li, A. Pei, K. Yan, Y. Sun, C.-L. Wu, L.-M. Joubert, R. Chin, A.L. Koh, Y. Yu, J. Perrino, B. Butz, S. Chu, Y. Cui, Science 358 (2017) 506–510.
[201] Y. Li, W. Huang, Y. Li, A. Pei, D.T. Boyle, Y. Cui, Joule 2 (2018) 2167–2177.
[202] M.J. Zachman, Z. Tu, S. Choudhury, L.A. Archer, L.F. Kourkoutis, Nature 560 (2018) 345–349.
[203] F. Sun, K. Dong, M. Osenberg, A. Hilger, S. Risse, Y. Lu, P.H. Kamm, M. Klaus, H. Markötter, F. García-Moreno, T. Arlt, I. Manke, J. Mater. Chem. A. 6 (2018) 22489–22496.
[204] X. Wu, J. Billaud, I. Jerjen, F. Marone, Y. Ishihara, M. Adachi, Y. Adachi, C. Villevieille, Y. Kato, Adv. Energy Mater. (2019) 1901547.
[205] H.-Y. Song, S.-K. Jeong, J. Nanosci. Nanotechnol. 16 (2016) 10583–10587.
[206] J. Zhu, L. Lu, K. Zeng, ACS Nano 7 (2013) 1666–1675.
[207] A.E. Semenov, I.N. Borodina, S.H. Garofalini, J. Electrochem. Soc. 148 (2001) A1239.
[208] X.-B. Cheng, C. Yan, X.-Q. Zhang, H. Liu, Q. Zhang, ACS Energy Lett 3 (2018) 1564–1570.
[209] Q. Zhao, X. Liu, S. Stalin, K. Khan, L.A. Archer, Nat. Energy. 4 (2019) 365–373.